

1
2
3 **NOVEL HAEMODYNAMIC STRUCTURES IN THE HUMAN GLOMERULUS**

4
5 **Neal CR¹, Arkill KP², Bell JS³, Betteridge KB⁴, Bates DO², Winlove CP⁵, Salmon**
6 **AHJ⁶, Harper SJ¹**

7
8 **¹Bristol Renal, Dorothy Hodgkin Building, University of Bristol, BS1 3NY, UK,**

9 **²Division of Cancer and Stem Cells, School of Medicine, University of Nottingham,**
10 **Queen's Medical Centre, Nottingham NG7 2UH, UK**

11 **³Cardiff Centre for Vision Science, Cardiff University, Cardiff, CF24 4HQ**

12 **⁴Nikon Imaging Centre, Guys Campus, Kings College London, SE1 1UL**

13 **⁵School of Physics, University of Exeter, Stocker Road, Exeter, EX4 4QL, UK**

14 **⁶Waitemata District Health Board, Auckland, New Zealand**

15
16 **Running title: Novel Human Glomerular Vasculature**

17
18 **Keywords: glomerular microcirculation, haemodynamics, mesangial collagen,**
19 **vascular chambers, conduit vessels**

20
21
22 CRN - Kidney perfusions, resin tissue processing, serial sectioning, resin section
23 reconstruction and 3D model construction, all measurements, plotting and statistics.
24 Preparation for confocal and multiphoton microscopy. Electron microscopy, model and
25 data interpretation, vascular chamber and conduit discovery, writing manuscript.

26 KPA - Reconstruction imaging, software assistance, multi-photon microscopy,
27 manuscript

28 JSB - Multiphoton microscopy and software, manuscript

29 KBB - Confocal microscopy and software, manuscript

30 AHJS, CPW, DOB, SJH – interpretation, grant support, manuscript

31
32 **Corresponding Author:**

33 Chris Neal. Bristol Renal, Dorothy Hodgkin Building, University of Bristol, BS1 3NY,
34 UK. +44 7599 169552. Chris.Neal@bristol.ac.uk

37 **Abstract**

38 To investigate human glomerular structure under conditions of physiological
39 perfusion we have analysed fresh and perfusion fixed normal human glomeruli at
40 physiological hydrostatic and oncotic pressures using serial resin section reconstruction,
41 confocal, multiphoton and electron microscope imaging.

42 Afferent and efferent arterioles ($21.5 \pm 1.2 \mu\text{m}$ and $15.9 \pm 1.2 \mu\text{m}$ diameter),
43 recognised from vascular origins, lead into previously undescribed wider regions
44 ($43.2 \pm 2.8 \mu\text{m}$ and $38.4 \pm 4.9 \mu\text{m}$ diameter) we have termed vascular chambers (VCs)
45 embedded in the mesangium of the vascular pole. Afferent VC(AVC) volume was 1.6
46 fold greater than Efferent VC(EVC) volume. From the AVC long non-branching high
47 capacity conduit vessels ($n=7$) (Con; $15.9 \pm 0.7 \mu\text{m}$ diameter) led to the glomerular edge
48 where branching was more frequent. Conduit vessels have fewer podocytes than filtration
49 capillaries. VCs were confirmed in fixed and unfixed specimens with a layer of banded
50 collagen identified in AVC walls by multiphoton and electron microscopy. Thirteen
51 highly branched efferent first order vessels ($E1; 9.9 \pm 0.4 \mu\text{m}$ diam.) converge on the EVC
52 draining into the efferent arteriole ($15.9 \pm 1.2 \mu\text{m}$ diam.). Banded collagen was scarce
53 around EVC.

54 This previously undescribed branching topology does not conform to the
55 branching of minimum energy expenditure (Murray's law), suggesting even distribution
56 of pressure/flow to the filtration capillaries is more important than maintaining the
57 minimum work required for blood flow. We propose that AVCs act as plenum manifolds
58 possibly aided by vortical flow in distributing and balancing blood flow/pressure to
59 conduit vessels supplying glomerular lobules. These major adaptations to glomerular
60 capillary structure could regulate haemodynamic pressure and flow in human glomerular
61 capillaries.

62

63 **Introduction**

64 The control of glomerular blood flow is crucial for maintaining efficient
65 ultrafiltration across the glomerular filtration barrier (GFB). Glomerular disease is
66 characterised by molecular and physiological perturbations and altered glomerular
67 haemodynamics (intraglomerular pressure and hyper-perfusion), however, most of the
68 models of glomerular haemodynamics in humans are based on experimental animals with
69 small glomeruli. A few studies have attempted to reconstruct the human glomerular
70 vascular network; a wax model of a human neonate glomerulus was reconstructed by
71 Johnston in 1899 (21) and in 1956 plastic glomerular vessels were reconstructed from
72 wax moulded outlines (6). These and later casting techniques render impressions of the
73 glomerular surface capillaries with deeper vessels remaining largely hidden.

74 More recent computational methods have revealed nodes and branching in rat and
75 human glomerular vasculature (33, 34, 47, 48, 53). The human reconstructions were
76 performed on $5 \mu\text{m}$ sections and/or on immersion fixed sources or only on small
77 glomerular regions and the few studies of the vascular pole of the human glomerulus
78 have used biopsy or cadaver recovered material (33, 56). To date, only one reconstructive
79 study has been published using perfusion-fixation of a human transplant kidney but at
80 elevated hydrostatic pressure (140mm Hg) where the authors chose a stereological
81 approach for vessel analysis rather than reconstruction (4).

82 Glomerular capillaries operate at relatively high pressure in life which in turn sets
83 urinary driving pressure in the Bowman's capsule and tubules producing tubular flow.
84 For instance, the human glomerular capillary hydrostatic pressure of 60 to 65 mmHg at
85 the afferent end (43) falls only 2-3mmHg to the efferent end. Countering this filtration
86 pressure is an afferent plasma colloid osmotic pressure of 25mmHg rising to 32mmHg at
87 the efferent end (1). As a result of filtration, urinary space hydrostatic pressure is 20-
88 25mmHg (61) pressurizing the proximal convoluted tubule producing flow through to the
89 collecting duct and the renal hilus. Thus, the function and structure of the whole nephron
90 relies upon the glomerular perfusion of an oncologically appropriate fluid at the correct
91 hydrostatic pressure to raise the right physiological pressures and flows in the tubules. In
92 biopsy/necropsy kidney specimens the absence of pressure during immersion fixation
93 results in the collapse of both the glomeruli and tubules. Fixing at the correct
94 physiological pressures (oncotic and hydrostatic) is therefore essential in investigating the
95 true 'functionally inflated' architecture of the glomerulus.

96 We have previously shown that 3D ultrastructural reconstruction of animal and
97 human glomeruli fixed under hydrostatic and oncotic physiological conditions allow the
98 detailed analysis of the GFB and the identification of novel structural features such as the
99 subpodocyte space (SPS)(39) One unexpected feature of light microscopic sections from
100 these resin embedded human glomeruli was the frequency of wide vessel regions at the
101 vascular pole when compared with rodent vascular poles implying different vascular
102 structure. No mention of any such difference could be found in any recent study of
103 human glomerular structure.

104 The haemodynamic requirements of rat and human glomeruli could shed light on
105 any differing evolved morphologies. For instance, if glomerular volume is assumed to
106 estimate perfused glomerular volume, this parameter does not scale in size with the
107 increase in afferent arteriolar conductivity between rodents and humans. The human
108 afferent arteriole has a conductivity 13 fold greater than that of the mouse ($14000\mu\text{m}^4$ vs
109 $1100\mu\text{m}^4$) but supplies a 23 fold larger glomerular volume [see Footnote 1]. Similarly, it
110 is 3 times as conductive as that of the rat ($4600\mu\text{m}^4$), while supplying a 5 fold larger
111 glomerular volume. If human glomerular morphology was simply scaled up from a small
112 rodent pattern, then afferent arterioles should be closer to $26\mu\text{m}$ in diameter instead of
113 $21\mu\text{m}$.

114 This study therefore aimed to investigate these novel wide vascular regions of
115 human glomeruli. How big were these regions? What was the wall structure and
116 dimensions and were there any other associated features? Did the region constitute a
117 wider region at the base of the afferent arteriole or a region of a thin walled capillary?
118 Could these structural differences be involved in compensating for a high glomerular
119 volume relative to the vascular input in human glomeruli? To address such questions,
120 human kidneys were perfuse fixed (at physiological hydrostatic and oncotic pressures)
121 and processed in such a way to reduce any accompanying tissue volume changes.
122 Glomerular vasculature was observed and reconstructions made from fresh or fixed
123 human kidney cortex using conventional light microscopy, confocal microscopy,
124 multiphoton microscopy and transmission electron microscopy.

127 **Methods**

128 **Fixation techniques**

129 Human kidney tissue was sourced (with full ethical approval and consent of next
130 of kin) from transplant kidneys (n=9) unused for technical reasons (eg poor major vessel
131 condition, damage at retrieval, tumour in the contralateral kidney). The transport solution
132 perfused through the kidney was Soltran (Potassium Citrate 0.86% w/v, Sodium Citrate
133 0.82% w/v, Mannitol 3.38% w/v, Magnesium Sulphate 1.0% w/v; Baxter Healthcare,
134 UK). Approximately 2-3 litres of the solution was perfused through the kidney
135 (200ml/minute, 120-140mmHg, 4°C) and then stored on ice. All other chemicals were
136 sourced from Sigma-Aldrich, UK.

137 Kidneys were transported in ice-cold flush media. Centimetre diameter fresh
138 cortical tissue was sampled from one pole for confocal and multiphoton microscopy and
139 stored in chilled (4°C) HEPES buffered Ringers solution. Smaller 1mm diameter tissue
140 pieces were taken from the cut surface and fixed in 2.5% glutaraldehyde in HEPES buffer
141 to serve as immersion fixed samples for TEM. At 4-10°C kidneys were debrided of
142 excess fat preserving the hilar components (renal artery, vein and ureter) and the sampled
143 polar area of the kidney was clamped off with a large locking forceps. The renal artery
144 was cannulated and the renal vein was cleared of any debris to allow outflow of perfusion
145 fluid.

146 To offset any hyperfiltration and hyperperfusion during fixation normal
147 hydrostatic and oncotic pressures were re-established by perfusing with an oncotically
148 balanced (25mmHg oncotic pressure) flush solution (50ml, 20°C). Colloid osmotic
149 pressures were measured using a modified Hanson osmometer. The flush solution
150 temperature was kept low to minimise autolytic/proteolytic activity. The hydrostatic
151 pressure in the renal artery was set at 100mmHg (similar to human mean arterial
152 pressure). After the flush bolus, 400ml of fixative was perfused through the kidney at the
153 same pressures and temperature. Flush solution concentration was (mM); NaCl(132), KCl
154 (4.6), MgSO₄ (1.3), CaCl₂ (2), HEPES (5), NaHCO₃ (25), D-glucose (5.5), 6.5% (w/v)
155 Ficoll 400. Fixative was the same as the flush solution but with 1.25% (w/v)
156 glutaraldehyde. The glycocalyx stain 0.5% lanthanum nitrate and 0.5% dysprosium
157 chloride was incorporated into the solutions in 2 kidneys.

158 1mm diameter samples of perfusion fixed kidney were taken from a medial sub-
159 capsular position and together with subcapsular immersion fixed samples were post-fixed
160 in osmium tetroxide, dehydrated with ethanol and processed into Araldite resin using
161 standard procedures.

162 To promote consistency in structural comparisons, measurement and observations
163 were limited on the glomeruli of the outer (subcapsular) cortex of kidneys in a medial
164 location half way between the poles (unless otherwise stated).

165

166 **Reconstruction of vascular poles from perfusion fixed kidneys**

167 Seven areas of resin embedded kidneys (n=4) which contained a high density of
168 glomeruli were identified in Toluidine Blue stained sections. These areas were serially
169 sectioned on a Reichert Ultracut microtome at 1µm thickness (2,095 sections
170 approximately 300 sections per area). From these serial section runs, 3 or 4 fully
171 sectioned glomeruli from each kidney were selected that clearly showed a vascular pole.
172 The afferent arterioles of each of the 14 glomeruli were identified by tracing to a larger
173 artery and/or the efferent arteriole traced to a peritubular position.

174 Digital micrographs (1,834) of serial sections of glomeruli (n=14) were made
175 using a x40 objective on a Nikon E400 microscope. Digital images were repositioned,
176 aligned, calibrated and measured using Image J software (NIH opensource ImageJ 1.46r
177 & 1.47o) and compiled into image stacks. Topological maps were made of the route and
178 diameter of the blood vessels coursing through the afferent and efferent parts of the
179 vascular pole.

180

181 **Resin section thickness calibration and glomerular diameter**

182 Measurement and reconstruction in the sectioning direction is reliant upon the
183 precision of the ultramicrotome mechanism controlling section thickness. To test the
184 accuracy of the ultramicrotome, glomeruli were assumed to be spherical and of similar
185 diameter in all directions. Glomerular diameter was measured in the sectioning direction
186 (z) as well as in the section plane (x,y). An ellipse was fitted over the largest glomerular
187 profile of a section image (x,y) and maximum and minimum diameters measured from
188 this, the results were pooled ($194.4 \pm 5.1 \mu\text{m}$ n=28). In the image stacks of a glomerulus
189 the first and last sections to contain the edge of glomerular blood vessels were found and
190 the number of intervening sections counted (202.4 ± 5.0 n=14). Assuming $1 \mu\text{m}$ section
191 thickness there was no significant difference between the estimates of glomerular
192 diameter from either method (t-test; $P=0.325$) and no correction was needed for section
193 thickness or measurements of length in the sectioning direction (z).

194 The glomerular diameters ($2r_x$ $2r_y$ $2r_z$) measured during the calibration of section
195 thickness were used to calculate glomerular volume ($V_G = 1.33 \pi r_x r_y r_z$).

196

197 **Glomerular and vascular orientation in resin section reconstruction**

198 Vascular pole recognition was most easily achieved in $1 \mu\text{m}$ serial resin sections
199 where the section plane was par-axial with the *vascular pole - urinary pole* axis of the
200 glomerulus, as a result reconstructed glomeruli were sectioned close to a paraxial plane.
201 The true diameters of any vessel profile was measured by searching the sequential images
202 for the appropriate vessel section and measuring vessel width (x,y). Section depth
203 diameter was taken from the limits of vessel walls in the sectioning direction (z). Vessel
204 lengths (between branch points for example) through the image stack were measured on
205 section if possible or by triangulating through the stack using sectioning depth and
206 horizontal 'on section' distance.

207 The three diameters of VCs (x,y and z) used to calculate the means in table 1 and
208 2 were further used to calculate afferent and efferent vascular chamber volume ($V_{AVC} =$
209 $1.33 \pi r'_{AVC} r''_{AVC} r'''_{AVC}$; $V_{EVC} = 1.33 \pi r'_{EVC} r''_{EVC} r'''_{EVC}$).

210 Bends between arterioles and VCs were assessed in resin section image stacks of
211 10 glomeruli by assessing the afferent and efferent arteriole axis vector and measuring
212 the change in angle into the VC axis vector (Fig.3A). This included measurements on
213 section and in the sectioning direction and triangulation in vessels moving at angles to the
214 section plane.

215

216 **Afferent first order (conduit) vessel ballooning in resin sections**

217 Any ballooning or hyperinflation of first order afferent (conduit) vessels was
218 estimated initially by comparing conduit diameters in areas of potentially high transmural
219 pressure gradient (conduit vessels with large areas of GFB, 0-60% mesangial cover) with

220 conduit diameters in areas of potentially low transmural pressure gradient (conduit
221 vessels with 80-100% mesangial cover). These data were further dissected in each
222 conduit vessel by subdividing the initial 0-60% mesangial cover group into 4 groups and
223 using the 80-100% mesangial cover group as a baseline to calculate the fold change in
224 diameter.

225

226 **Podocyte cell body coverage of conduit vessels**

227 Podocyte cell body (PCB) coverage on the urinary side of conduit vessels was
228 estimated by measuring length of GFB in a vessel image covered by a visible podocyte
229 cytoplasmic region and the accompanying areas where no cell body was apparent. This
230 was compared with similar measurements from filtration capillaries.

231

232 **VC recognition in single resin sections**

233 To test whether evidence of VCs could be seen in single sections of glomeruli
234 (being the more common way of looking at human biopsy glomeruli) the occurrence of
235 widened vasculature at the vascular poles was assessed in single sections of renal cortex.
236 In an additional 13 resin-embedded human kidneys, immersion and perfusion fixed single
237 cortical sections (1µm thick) were stained with Toluidine Blue. Glomerular sections
238 showing vascular poles were assessed for the frequency of vascular widening around the
239 poles. Width was assessed by placing an ellipse around widened vascular profiles and
240 taking the minimum diameter to eliminate oblique vascular diameter measurements.

241

242 **Confocal and multiphoton light microscopy on fresh kidney slices**

243 Aqueous fresh and fixed kidney was observed using confocal and multiphoton
244 microscope techniques.

245 A Nikon confocal microscope (Nikon Eclipse Ti) was set to image fixation
246 induced autofluorescence (FIA). Millimetre and sub millimetre thick fixed renal cortical
247 slices were washed in HEPES Ringer solution and the autofluorescent signal (FIA) at
248 488nm wavelength was used to image and obtain z stacks from glomerular vascular poles
249 of up to 100µm depth from the cut surface.

250 Using a multiphoton microscope, two fresh and two fixed unstained slices of renal
251 cortex, were imaged as previously described (2). Two imaging modes were applied,
252 fibrous collagen was visualised using second harmonic generation (SHG) and elastin
253 from its intrinsic two photon fluorescence (TPF) along with any background
254 fluorescence. TPF and SHG images were obtained using a modified confocal microscope
255 (FluoView IX71 and F300, Olympus). Signal was produced using the 800 nm output of a
256 mode-locked Ti:sapphire laser (Mira 900-D, Coherent Inc) pumped by a 532 nm solid
257 state laser (Verdi V10, Coherent Inc.). The pulsed laser had a pulse width of 100 fs and a
258 repetition rate of 76 MHz. The light was focused on to the sample using a 60X 1.2 NA
259 water immersion objective (UPlanS Apo; Olympus). Signal was collected in the epi-
260 direction using the objective lens and separated from the laser fundamental using a long
261 pass dichroic mirror (670dcxr; Chroma Technologies). The signal was then passed
262 through two filters (for TPF: CG-BG-39 and F70-500-3-PFU; and for SHG: CG-BG-39
263 and F10-400-5-QBL; CVI Laser) before being focused on a photomultiplier tube (R3896,
264 Hamamatsu). Each 1024×1024 pixel image took 29 seconds to acquire, meaning a stack

265 of 100 images, each separated in the z-direction by 1 μm , took approximately 50 minutes
266 to complete.

267

268 **Electron microscopy**

269 From 1 μm Resin sections of renal cortex showing identifiable VCs, further
270 sections were cut at 70-100nm thickness and stained with 10% Phosphotungstic acid (10
271 minutes). Sections were viewed and digital images taken on a Tecnai T12 (FEI UK Ltd).

272

273 **Calculation of vascular resistance**

274 The resistance to flow along the terminal part of the arterioles will change as
275 blood enters AVCs and conduits, and exits EVCs. Assessing such resistances may give a
276 better understanding of how blood flow will be affected by VCs and conduits, a correlate
277 of total conduit resistance per unit length (R'_{Con}) was derived from the Poiseuille equation
278 (see Appendix 1)

279

$$280 \quad R'_{\text{Con}} = \frac{1}{r_{\text{Con}}^4 \cdot n_{\text{Con}}} \quad \text{Eq.1}$$

281

282

283 Where r_{Con} is the mean conduit vessel radius and n_{Con} is the number of conduit
284 vessels merging from an AVC. R'_{Con} provides a value that scales proportionately with
285 total vascular resistance per unit length. Similarly a correlate of first order efferent (E1)
286 resistance per unit length (R'_{E1}) was estimated from $1/r_{\text{E1}}^4 n_{\text{E1}}$ and arteriole resistance per
287 unit length (R'_{AA} , R'_{EA}) was calculated from $1/r_{\text{AA}}^4$ and $1/r_{\text{EA}}^4$.

288

289 **Statistics**

290 Data were represented throughout as either mean \pm standard error of the mean or
291 as median (interquartile range). Excel was used for collating data and initial statistics,
292 Prism software (Graphpad Software Inc.) was used for statistical analysis generating
293 histograms, correlations, parametric and non-parametric tests.

294

295 **Results**

296

297 **Glomerular structure from resin serial section image stacks**

298 **Glomerular Arterioles**

299 Assigning afferent and efferent labels to arterioles was accomplished by tracing
300 the origin of these vessels in the serial section image stacks. Branches of cortical radial or
301 interlobular arteries (38, 58) were traced to the afferent arterioles (Fig.1) and efferent
302 vessels showed a characteristic peritubular branching course on emerging from
303 glomeruli.

304 Afferent and efferent arteriole wall thickness were significantly different
305 ($6.6 \pm 0.3 \mu\text{m}$, $3.0 \pm 0.1 \mu\text{m}$ respectively, paired t-test $p < 0.0001$ $n=7$) as were afferent and
306 efferent luminal diameter ($23.2 \pm 1.8 \mu\text{m}$, $17.6 \pm 2.0 \mu\text{m}$ respectively, paired t-test $p=0.02$
307 $n=7$). Wall thickness being a better predictor of arteriole type than luminal diameter. No
308 correlation was found between the afferent (R'_{AA}) and efferent (R'_{EA}) arteriole resistance
309 measure (Tab.3 $R^2 = 0.033$ $P=0.53$).

310 The efferent picture was confused by multiple efferent arterioles in 4 out of 14
311 glomeruli. Major efferent arterioles have been shown in table 2, the extra 1 to 3 minor
312 efferents were in series or parallel with EVC and were 4.6-8 μ m diameter with one
313 11.5 μ m in series with an efferent VC. No extra afferent arterioles were seen.

314

315 **Reconstruction of VCs and 1st order vessels**

316 All 14 glomeruli (4 kidneys) analysed from image stacks of 1 μ m resin serial
317 sections showed afferent and efferent widening of the arterioles, resulting in vascular
318 chambers (VCs) embedded in the mesangium of the vascular pole (Fig.2, see
319 supplemental video 2a and 2b for full image stacks). Some afferent VCs (AVCs)
320 protruded into a hilar or juxta-glomerular position (sections 198 & 209, Fig.2B).

321 Vascular width and connectivity is illustrated in a scale diagram in figure 3A,
322 (measurements from tables 1&2). To summarize, the 21 μ m diameter afferent arteriole
323 (AA) leads into an ellipsoidal afferent vascular chamber (AVC; 49x48x32 μ m) which
324 branches into on average 7 first order afferent vessels of 16 μ m diameter we have termed
325 conduit vessels (Con; Fig.2A, B, Fig.3A, Tab.1). These vessels had secondary vessels
326 (A2) emerging at spacings of 32.8 μ m (median), with 41% of branches intervals between
327 A2 greater than 40 μ m with a quarter of these above 100 μ m (Fig.4A). Conduit branches
328 into A2 were more frequent distal to the AVC at the glomerular edge (Fig.2B. &
329 supplemental video 2a and 2b). Conduit vessels coursed through mesangium and then
330 either through the centre of the glomerulus or peripherally over the glomerular surface
331 before branching into capillary networks (Fig.2A & B) [Supplementary videos S2c and
332 S2d (Fig.2B as a reconstructions)].

333 At the efferent end of the filtration capillary network first order efferent vessels
334 (E1) were more numerous (13 v. 7) and narrower than conduits (10 μ m v. 16 μ m diameter;
335 Fig.4B; Tab.1&2). Secondary efferents (E2) merged at 15 μ m intervals into 13 first order
336 vessels (E1) (Figs.2A, B & 3A). Only 4% of E2 branch intervals on E1 vessels were
337 above 40 μ m - (Fig.4A). E1s converged into an efferent vascular chamber (EVC;
338 46x43x26 μ m) in turn disgorging into a 16 μ m diameter efferent arteriole (EA; Figs.2A, B
339 & 3A, Tab.2).

340 In 10 of the 14 glomeruli where the orientation of afferent and efferent arterioles
341 on entry into the VCs could be easily assessed, the AA bent 60° off its straight track into
342 the AVC (AA/AVC angle = 120±6°), similarly, the EA bent 71° off track into EVC
343 (EA/EVC angle = 109±7° Fig.3A).

344

345 **VC and glomerular size**

346 AVC volume ($V_{AVC} = 41\pm 5 \times 10^3 \mu\text{m}^3$) was 1.6 fold greater than EVC volume
347 ($V_{EVC} = 28\pm 7 \times 10^3 \mu\text{m}^3$), with no correlation between them ($R^2 = 0.164$ P=0.152). V_{AVC}
348 varied over a greater size range (15-70x10³ μm^3) with V_{EVC} more conserved (12 out of 14
349 between 10-40x10³ μm^3). Both V_{AVC} and V_{EVC} correlated significantly with V_G (Fig.4C,
350 D, Tab.4), V_G being 100 fold larger than V_{AVC} and 150 fold larger than V_{EVC} 150. This
351 implies a relationship of both the input the output manifold with the magnitude of the
352 perfused volume.

353 If the glomerular and VC volume (Fig.4C, D) correlation is extrapolated back
354 from larger glomeruli then a minimal VC volume can be reached where the volume
355 describes a mere continuation of the attached arteriole (Fig.3B). Accordingly, a

356 cylindrical minimum VC volume was calculated using average VC length (L) and
357 arteriole radius (r), a minimum AVC volume of $1.57 \times 10^4 \mu\text{m}^3$ would occur at a V_G of
358 $2.2 \times 10^6 \mu\text{m}^3$ (Fig.4c). Similarly, a minimum EVC volume of $0.75 \times 10^4 \mu\text{m}^3$ would occur at
359 a V_G of $2.9 \times 10^6 \mu\text{m}^3$ (Fig.4D). Translating V_G into glomerular diameter, VCs would be
360 minimal (a continuation of the arteriole) in human glomeruli below 160-180 μm diameter
361 (i.e. $V_G = 2 - 3 \times 10^6 \mu\text{m}^3$).

362

363 **Conduit podocytes**

364 In resin section image stacks spanning a conduit vessel, we noted a significant
365 lack of coverage of podocyte cell bodies (PCB) over the GFB surface (e.g. Fig.2A Con in
366 sections 312 & 329; Supplemental 2a & 2b). Narrower, shorter first order efferent vessels
367 (E1) were embedded in mesangium adjacent to the EVC and so had zero podocyte
368 coverage (e.g. Fig.2B E1 in sections 249, 258 & 266). PCB area coverage was estimated
369 in GFB conduit regions (n=10, i.e. Fig.2; GFB.Con Fig.3) and small filtration capillary
370 regions (n=22) from 4 human glomeruli. Conduit vessel PCB area coverage was halved
371 compared with small filtration capillaries ($29 \pm 3\%$ v. $55 \pm 3\%$; ttest - $P < 0.0001$; Fig.5B).

372

373 **Conduit mesangial support**

374 Conduit vessels proceed from a central glomerular region with mesangium on all
375 sides (Fig.3A Mes.Con) to regions with less mesangial attachment and areas of filtration
376 barrier (Fig.3A GFB.Con). Appendix 2 shows that moving from mesangial supported
377 regions of conduit to regions where this support is replaced by GFB more than doubles
378 the hoop stress tending to inflate or expand the vessel wall. To test if the GFB conduit
379 regions showed any ballooning due to lack of mesangial support, conduit vessel
380 diameters measured in 13 glomeruli (resin reconstruction method) were the same in high
381 (80-100% mesangial cover) and low mesangial cover regions overall
382 ($17.7 \pm 0.8 \mu\text{m}$, $17.9 \pm 0.4 \mu\text{m}$ respectively, paired t-test, n=61, p=0.28). However, after
383 further division of the low mesangial cover data set, conduit vessels with the lowest
384 mesangial cover (<15% mesangium, >85% GFB) showed significant inflation of 7%
385 compared to high mesangial cover regions close to the AVC (paired t-test $P=0.04$,
386 Wilcoxon $P=0.04$; Fig.5A).

387

388 **Vascular Resistance and volume relationships**

389 Since Poiseuille flow conditions do not apply to an ellipsoidal chamber manifold
390 with many branches, the vascular resistance per unit length could not be calculated for
391 VCs, therefore their capacity, V_{AVC} or V_{EVC} , was compared with glomerular vessel
392 resistance parameters. Glomerular volume (V_G) was used as a correlate of perfusion
393 volume and compared with the resistance parameters.

394 R'_{AA} did not correlate with any of the other R' parameters or V values, no
395 correlation was found between R'_{AA} for afferent arterioles and V_{AVC} ($R^2 = 0.014$,
396 $P=0.68$) or V_G which it supplies ($R^2 = 0.065$, $P=0.38$) (Tab.3). From the afferent VC
397 there was a significant negative correlation between V_{AVC} and R'_{Con} ($R^2 = 0.327$,
398 $P=0.033$; Fig.5C; Tab.3) showing that as the input manifold gets larger the supply
399 conduits to the filtration capillary regions get proportionally more conductive (wider).

400 On the efferent side there was no similar correlation between efferent first order
401 vessels R'_{E1} and V_{EVC} ($R^2 = 0.088$, $P=0.303$) though both of these correlated with V_G

402 implying a link with perfusion volume. No correlation was found between R'_{EA} and V_{EVC}
403 ($R^2 = 0.22$, $P=0.094$) but R'_{EA} does correlate inversely with V_G ($R^2 = 0.47$, $P=0.007$;
404 Fig.5D, Tab.3) and directly with both first order afferents (R'_{Con}) and efferents (R'_{E1}).

405 Table 3 summarizes the capacity and resistance parameter correlations in the
406 human glomerulus; strikingly, R'_{AA} remains independent of all glomerular parameters but
407 all other glomerular vascular entities appear fluid dynamically tied together.

408

409 **VC in single resin sections.**

410 Single sections of immersion and perfusion fixed kidney (n=13) revealed
411 randomly orientated profiles of glomeruli with vascular poles (n=177). There was no
412 significant difference in the occurrence of vascular widening at the vascular poles
413 between immersion and perfusion fixed glomeruli or between juxta medullary (JM) and
414 subcapsular (SC) glomeruli (Fig.6A). Analysis of all glomeruli together where no
415 discrimination was made in glomerular position (JM/SC) in 8 immersion fixed tissues
416 revealed vascular widening in $53\pm 5\%$ of vascular pole sections. Overall frequency was
417 $60\pm 4\%$ for vascular widening in single sections of glomerular vascular poles.

418 The widened vascular regions found at SC vascular poles were $28.5\pm 3\mu\text{m}$ and
419 $30.7\pm 2.1\mu\text{m}$ (minimal diameter) after immersion or perfusion fixation respectively and
420 represented randomly oriented sections of presumably both vascular chambers. This lack
421 of collapse shows that VCs appear to remain open even when the vascular pressure is
422 reduced during fixation. The full morphology of JM vascular chambers remains to be
423 investigated with serial sections.

424

425 **VC imaged by confocal and multiphoton microscopy**

426 Using a combination of fixation induced autofluorescence (FIA), two photon
427 fluorescence (TPF) and second harmonic generation (SHG) modes, AVC could be seen
428 with attached wide conduit vessels and AA in both fixed and fresh kidney slices (Fig.7).
429 EVC was more difficult to observe with narrower blood vessels (E1) emerging from
430 them. Measurements of recognised structures show similar dimensions using these
431 optical sectioning methods and resin section reconstruction methods (Tab.4).

432 In addition to morphology SHG can detect collagen without the need for fixation
433 or labelling. Coherent emission in SHG mode in unfixed glomeruli revealed a signal
434 consistent with banded collagen which when overlaid with co-registered TPF images was
435 positioned in the AVC walls (Fig.7, Supplemental video S3). The collagen sheath
436 extended throughout the AVC and a short distance along the attached conduit vessel
437 walls. A similar banded collagen signal was also seen in fixed tissues. TPF imaging
438 showed fresh glomeruli with extensive vessel collapse in the filtration networks but VCs
439 appeared resistant to collapse as was found with resin section reconstruction and resin
440 single sections.

441

442 **VC wall appearance under electron microscopy**

443 No visible sign of collagen fibres could be seen in the $1\mu\text{m}$ light microscopy resin
444 sections. Electron microscopy sections of AVC showed regions of banded collagen fibres
445 in the surrounding mesangial matrix. The banding was sparse and poorly stained
446 ($30\pm 1\text{nm}$ band spacing) and width of the fibres ($30\pm 2\text{nm}$) in this partial sheath was
447 consistent with Collagen I and III (Fig.8a-d). The collagen bundles extended to a depth of

448 4µm from the VC surface (Fig.8C; Tab.4). The endothelial lining of AVC contained few
449 fenestrations together with cellular distortions and membrane blebs (Fig.8C), unlike the
450 abundant fenestral density of the filtration capillaries.

451
452
453

454 **Discussion**

455

456 **Vascular chambers**

457 Human glomerular microvascular architecture is not as depicted in current texts.
458 The vascular layout developed over the last 170 years since William Bowman (5) is of a
459 single afferent arteriole which branches until filtration capillaries are reached. These
460 filtration capillaries converge to form a single efferent arteriole conveying blood to the
461 peri-tubular vasculature. This classic picture has been built up from biopsies or
462 necropsies of mammalian kidney.

463

464 In human glomeruli both arterioles exhibit vascular widenings more frequently
465 associated with low pressure veins (venous sinuses of the brain) or with large arteries
466 (carotid sinus). However, the glomerular VCs are high pressure arteriolar afferent and
467 efferent chambers with multiple openings, the closest definition in physical terms is a
468 plenum manifold (plenum - a chamber containing pressurized fluid to control
469 distribution; manifold - a pipe or chamber branching into several openings).

470 Plenums and manifolds in industry stabilize, distribute or balance fluid flow
471 through multiple inlets and outlets (i.e. inlet and exhaust manifolds on internal
472 combustion engines). Therefore, our initial hypothesis for glomerular vascular chambers
473 is that they function to balance the pressure and/or flow through the intervening filtration
474 regions without the need for conventional branching within the confined space of the
475 glomerulus. These haemodynamic considerations are not relevant in smaller rodent
476 glomeruli with smaller perfusion volumes relative to arteriolar conductivity (see
477 introduction).

478 These VC manifolds persist in the glomerulus despite pressure changes, VC walls
479 are resistant to collapse during immersion fixation or when observed fresh at zero
480 pressure. The VC position at the vascular pole allows mesangial structural support and
481 Collagen I/III appears to provide (additional) structural integrity. The physiological
482 significance of this collapse resistance is not yet clear.

483 Collagen III has been observed in glomeruli of collagen nephropathies (7, 14)
484 with collagen III in mesangium and/or capillary walls. No report could be found of
485 Collagen I or III in mesangium of normal glomeruli and this report is the first to find
486 banded Collagen (I and/or III) in normal glomeruli close to the vascular pole. Banded
487 collagen has previously been found in kidney cortex, where 30nm fibres showed hybrid
488 labelling with Collagen I and III (13), however, the identity of VC wall banded collagen
489 remains to be confirmed by immunohistochemistry.

490

491 VCs appear to be ubiquitous in the adult kidney. We confined resin section
492 reconstructions in this study to subcapsular glomeruli to surmount any size difference
493 between subcapsular and juxtaglomerular glomeruli seen in humans and other species

494 (17, 34, 51, 55, 58) Evenso, the resin single section work shows a surprisingly similar
495 occurrence of vascular widening in 50-60% of vascular pole glomerular profiles (Fig.6),
496 implying that VCs exist in both cortical locations with similar sized VCs in both juxta-
497 medullary and subcapsular glomeruli.

498

499 **Afferent and efferent arterioles**

500 No previous study has measured the diameter of fully opened human glomerular
501 arterioles perfusion fixed at their operating pressures. Previous human AA diameters vary
502 from 13-16 μ m (18) to diabetic biopsy diameters of 29 μ m for AA and 19 μ m for EA(44).
503 Other than biological variability, this range of arteriolar diameter is likely due to: volume
504 changes in tissue processing, oblique sections of vessel or low pressure fixation
505 producing collapsed profiles (for example; Tab.4 fresh AA - 13.8 μ m; Fig.1 in ref.(45)).
506 These problems appear minimized with the fixation and resin embedding techniques of
507 this paper.

508 A correlation between afferent arteriolar diameter and mean glomerular capillary
509 area has previously been seen as consistent with loss of autoregulation (18). Here a
510 correlate of AA resistance per unit length (R'_{AA}) did not scale with any other glomerular
511 parameter measured including R'_{EA} (Tab.3) preserving the independent autoregulatory
512 control of AA. In contrast EA resistance per unit length (R'_{EA}) was inversely correlated
513 with V_G (Fig.5D; Tab.3), and correlating remarkably with R'_{Con} at the afferent end
514 (Tab.3). Unlike AA, EA is linked in fluid dynamic terms with the Glomerulus it drains.

515

516 **Conduit vessels**

517 The first order afferent vessels or conduits were noted by Bowman in 1842, with
518 2 to 8 branches which visibly 'subdivide only once or twice as they advance over the
519 surface of the ball' (5). The few buried deep inside the glomerulus unseen by Bowman
520 may explains the result of 2 to 11 seen in this current study. We also confirm the luminal
521 width of these first order afferent vessels as being as wide as the efferent arteriole (21).

522 Conduit vessels show fewer branches than their efferent counterparts but branch
523 frequency increases at the start of perfusion regions often at some point on the glomerular
524 periphery (Fig.2). No previous branch data exists for these vessels however, the
525 interbranch length for all rat glomerular vessels at $26.3 \pm 24.9 \mu\text{m}(\text{SD})$ (48) is between the
526 medians, 32.8 μ m (conduit afferent) and 15 μ m (efferent) of the skewed distributions
527 found here.

528 Conduit vessels close to the AVC are embedded in mesangium, those distal to the
529 AVC have a GFB. While detailed conduit ultrastructure remains to be confirmed, no
530 aberrant GFB capillary morphology has been noted in all our studies of normal human
531 glomeruli (data not shown). It appears that conduit GFB is similar to filtration capillary
532 GFB except for the scarcity of podocyte cell bodies on the conduit GFB surface. It
533 remains to be determined if conduit podocytes are just responding to local conditions or
534 are a sub-population of conduit podocytes with the extra-long major processes necessary
535 to cover the GFB area in foot processes.

536 The GFB is known to remain intact and expand under excess pressure (25, 27)
537 and conduit vessels with a 86-100% GFB - or a sparse 0-14% mesangial attachment
538 around the circumference showed diameter expansion by 7% compared to conduit vessels
539 surrounded by and embedded in mesangium (Fig. 5A) - not enough GFB expansion to

540 explain podocyte cell body free areas on the conduit vessels but below the damaged
541 ‘giant capillary’ inflation levels previously reported (25). Conduit inflation might be
542 expected considering the reduced podocyte coverage, thin walls and wide diameter and
543 estimates of wall forces show conduit vessels with a high proportion of GFB and low
544 mesangial attachment are the most susceptible to hoop stress of all glomerular vessels
545 (Appendix 2). This marks conduits as a target in hypertensive disease and hoop stress
546 failure has been observed in rat primary afferents (equivalent to conduits) due to
547 glomerular hypertension (with marking albuminuria and glomerulosclerosis) (26).

548 The subpodocyte space, identified under podocytes (39) should be present under
549 conduit podocyte cell bodies (awaiting EM confirmation). Incidentally, the light
550 microscopy derived filtration capillary podocyte cell body (PCB) area coverage of 55%
551 of the GFB fits well with the electron microscopy derived subpodocyte space coverage of
552 60% for filtration capillaries found previously (41, 50) suggesting most of human
553 subpodocyte space is under the podocyte cell body.

554

555 **Other evidence for vascular chambers and conduits**

556 Reconstructed rat glomeruli do not show vascular chambers (48). We confirmed
557 these findings by reconstructing rat glomeruli with Serial Block Face Scanning Electron
558 Microscopy (data not shown) and also found no evidence of VC.

559 Mammalian arterioles can widen pathologically (32), for instance, mesangiolytic
560 can remove mesangial support causing glomerular vessel aneurysms (35) but such
561 features would not be as highly conserved in shape or have an organized collagenous
562 support as seen in VC found here. Bowman also noted in the larger horse glomerulus that
563 afferent arterioles dilate on the surface prior to dividing but not in human glomeruli (5)
564 we show here that human glomerular vascular dilations are subsurface and would have
565 been invisible to Bowman. The modern conventional description merely reports that the
566 afferent arteriole branches into the glomerular capillary network (22).

567 VCs may not be present in all human glomeruli, during development, glomerular
568 capillaries arise from one dilated vessel (11) and neonate vascular widening has been
569 shown prior to the five first order afferent branches (21) although this has been ascribed
570 to a vessel remnant from the developing nephron (11). Interestingly, the glomerular
571 diameter increase in children from 112 μm (birth) to 167 μm (15years) (34) and VC
572 scaling with V_G shows that VCs may not exist in child glomeruli which are below 160-
573 180 μm diameter, providing these glomeruli follow the adult glomerular correlation (Fig.
574 3B & 4C,D). Conduit vessel resistance (R'_{con}) also scales with V_G , whether this
575 correlation continues in smaller (child) glomeruli or whether the primary afferents in
576 children even constitute ‘conduit’ vessels needs evaluation.

577 Renal biopsies do occasionally show evidence of VCs and conduit vessels in
578 section, a survey of images in biomedical journals reveal light micrographs showing a
579 15 μm conduit vessel and 20 μm VC (20), a 30 μm diameter VC (52) and VCs at both
580 efferent and afferent ends (44). However, without the context of a serial section stack
581 these micrographs remain as widened vascular profiles.

582 VCs could be artefacts of processing volume changes, however, glomerular
583 diameters (~200 μm) derived here were between immersion fixed (160 - 170 μm) (10, 31)
584 and autopsy diameters (260-270 μm) (8) and closely match in vivo ultrasound values of

585 200µm (15, 23), suggesting glomerular volume changes during processing were minimal
586 overall.

587 Wide profiles at the vascular pole in singles sections can be dismissed as
588 collapsed vessels. Put simply, an afferent arteriole terminus of 21µm diameter with a
589 circumference of 66µm could conceivably collapse to a flattened squashed-circle profile
590 approximately 30µm wide which if sectioned longitudinally would fit exactly with the
591 28-30µm wide profiles measured, however, 60% of randomly oriented single sections of
592 vascular poles all showed these wide vascular regions - far too frequent for the collapse
593 argument. Additionally, in this study vessel collapse was seen in filtration capillaries in
594 fresh glomeruli (multiphoton microscope: Supplemental Fig. S3) but with VCs held open.
595 VCs are not collapse artefacts but stiff walled vascular structures.

596

597 **The Murray relationship**

598 The relationship between branching vessel diameters was derived by Murray on
599 the principle of minimum work for blood flow (36, 37) where the radius cubed of the
600 parent vessel equals the sum of the cubes of the daughter vessel radii. The Murray
601 relationship holds for arteries and venules of rat kidney down to the afferent arterioles
602 and venules leading away from the tubular networks (42), but it is not known if it
603 continues into the glomerulus. The Murray relationship in whole human kidney also
604 remains to be assessed.

605 A Murray constant (K) was calculated for each set of vessels leading into and
606 away from human glomerular VCs in all 14 glomeruli reconstructed from resin sections:

607

$$608 \quad K = r^3 n_V \quad \text{eq.2}$$

609

610 Where n_V is the number of vessels and r is the radius. Using r_{AA} , r_{AVC} , r_{Con} , r_{E1} ,
611 r_{EVC} , r_{EA} and appropriate n to calculate K , the Murray relationship breaks at the VCs and
612 the first order vessels (conduit and E1 vessels; Fig.6B), where daughter vessels do not
613 have the same Murray constant as parent vessels.

614 This is an exception to Murray's Law – a plenum/manifold exception, where flow
615 distribution from a single arteriole provides a high pressure distributive flow into many
616 glomerular lobes in a short distance. An estimate of K values for second order afferent
617 vessels (A2 in 2 glomeruli) showed that K may return to the value predicted by the
618 afferent arteriolar radius after skipping the VC and conduit vessels (Fig.6B). Other
619 Murray's law exceptions occur where a higher surface area is required in the exchange
620 vessels of an organ, for instance alveolar capillary networks (59).

621 The possible mechanisms producing a set of vessels following Murray's law
622 includes an endothelial transducer triggering remodelling after a shear force threshold
623 was exceeded(46). Altering the threshold could induce the vessel diameter changes seen
624 here. However, the Murray relationship requires laminar flow through vessels and the
625 haemodynamic flow will be complex from an afferent arteriole into an ellipsoidal
626 vascular chamber with several outlets.

627

628 **VC haemodynamics**

629 If glomerular volume is used as a measure of perfusion capacity, it rises and falls
630 along with the size of the AVC and the EVC (Fig.4 C&D). Larger AVCs feed more

631 blood to larger glomerular filtration regions and thence to larger EVCs. As the size
632 increases the resistance of the conduit vessels, E1 and EA (not AA) falls to accommodate
633 the flow (vessels get wider in proportion to Poiseuille flow) (Fig.5 C&D). All of the
634 major vessels of the human glomerulus past the afferent arteriole are linked in some way
635 in terms of flow and capacity (Tab.3). How would flow progress from laminar flow in an
636 afferent arteriole through the AVC to the conduit vessels? And similarly from efferent E1
637 vessels through EVC to the efferent arterioles?

638 A clue to VC flow characteristics comes from the kinks and bends in AAs. One
639 constant feature of the glomeruli analysed is the bend as the afferent arteriole enters the
640 AVC. These bends can be readily seen in the glomeruli of figures 1, 2A and 2B
641 (supplemental videos 2a and 2b) and showed an average 60° deviation from a straight
642 path. The fluid flow at a bend in a channel is known to induce vortices (49), we
643 hypothesize that the summation of all bends in an afferent arteriole (i.e. see bend from
644 interlobular –AA junction in Fig.1) could induce a single major vortex in the AVC
645 possibly aiding distributive flow centrifugally into conduit vessels.

646 If such a vortex with its axis in the midline of the AVC adopts the properties of a
647 “rigid-body” or “rotational” vortex, then the pressure at the AVC edge at the conduit
648 vessel openings would depend both on the hydrostatic pressure and the dynamic pressure
649 (set by the angular momentum of the moving fluid – $\frac{1}{2}\rho\omega^2$, where ρ =density; ω = angular
650 velocity). Crucially however the dynamic pressures within this form of vortex are
651 uniform (3).

652 We speculate that in health the AVC and the complex (vortical) fluid movement
653 within it, may ensure a uniform driving pressure into the conduit vessels – maximising a
654 uniform distribution of flow to each of the glomerular lobules. The loss of this equalising
655 distributary mechanism through microvascular disease, mesangial proliferation occluding
656 the AVC, hyperperfusion or immunological injury, could potentially result in localised
657 hyperfiltration and excess shear stress in some glomerular segments with stasis in others.
658 This has implications for glomerular disease in which only some perfused regions of the
659 glomerulus appear to have sustained sclerotic/fibrotic damage (eg FSGS) while adjacent
660 lobules appear normal.

661 The structure of the efferent vascular chamber, with many microvessels
662 converging on a chamber, lends itself to the development of an irrotational vortex (plug
663 hole vortex) balancing EVC pressure gradients and promoting balanced removal of blood
664 from the glomerular tuft (3).

665

666 **Conclusion**

667 We show for the first time in human glomeruli that clearly defined afferent
668 arterioles lead into afferent vascular chambers of ellipsoid shape and structure embedded
669 in the mesangium of the glomerular vascular pole and ensheathed in collagen fibrils.
670 These chambers are plenum manifolds with many emergent relatively unbranched wide
671 blood vessels or conduits conveying blood to the periphery of the glomerulus. Branching
672 frequency increases at the end of the conduits leading to filtration capillary networks
673 which lead back to smaller efferent vascular chambers in the mesangium of the vascular
674 pole and then the efferent arteriole. The conduit vessels are sparsely covered with
675 podocytes, and conduit fluid resistance scales with the size of the afferent vascular
676 chambers. Both vascular chambers scale with glomerular capacity suggesting absence of

677 vascular chambers in glomeruli below 160µm diameter (the glomeruli of children).
 678 Resistance correlates of first order afferent (conduit) and efferent vessels and efferent
 679 arterioles (but not afferent arterioles) scale together and inversely with glomerular
 680 volume. We propose that all these structures represent a large glomerulus adaptation
 681 allowing even haemodynamic flow distribution and pressure balance across the many
 682 lobes of a human glomerulus.

683
 684
 685
 686
 687

688 **Appendix 1.**

689

690 **Vascular resistance**

691 *The vascular resistance to flow will change as blood flows along AA into AVCs*
 692 *and conduits and later pools in EVCs before flowing into EA. To better understand how*
 693 *blood flow is affected by the changing morphology a correlate of vascular resistance*
 694 *R'_{Con} was derived from the Poiseuille equation using vessel radii and vessel number. For*
 695 *VCs the flow will be complex and non-laminar in the spheroidal shape and so the*
 696 *Poiseuille equation could not be used so VC volume was used as a measure of VC*
 697 *capacity.*

698

699 **Resistance changes in arterioles and conduit vessels**

700 *For conduit vessel resistance ($\sum R_{Con}$) coming out of the afferent VC where R_{Con3}*
 701 *is the resistance of the 3rd conduit vessel in parallel:*

702

$$703 \quad \frac{1}{\sum R_{Con}} = \frac{1}{R_{Con1}} + \frac{1}{R_{Con2}} + \frac{1}{R_{Con3}} \dots \frac{1}{R_{Conn}} \quad \text{eqA1.1}$$

704

705
 706 *For n_{Con} similar conduit vessel resistances R_{ConX}*

$$707 \quad \frac{1}{\sum R_{Con}} = \frac{n_{Con}}{R_{ConX}} \quad \text{eqA1.2}$$

708

709

710
 711 *For fluid of viscosity η , the resistance to flow through a tube of length L is inversely*
 712 *proportional to the 4th power of the radius (Poiseuille's law), similarly:*

713

714

$$715 \quad R_{ConX} = \frac{8 \eta_{Con} L_{Con}}{\pi r_{Con}^4} \quad \text{eqA1.3}$$

716

717

718 *Where L_{Con} is conduit vessel length and r_{Con} the mean conduit vessel radius. If the*
 719 *viscosity of the blood flowing through VC and attached vessels (η_{Con}) is assumed not to*

720 change (low filtration into mesangium in these vessels) then η_{Con} with π and δ can be
 721 combined into a constant k_{Con} :

$$722$$

$$723 \quad R_{ConX} = \frac{k_{Con} L_{Con}}{r_{Con}^4} \quad \text{eqA1.4}$$

$$724$$

$$725$$

726 Combining equation eqA1.2 and eqA1.4:

$$727$$

$$728 \quad \frac{1}{\sum R_{Con}} = \frac{r_{Con}^4 n_{Con}}{k_{Con} L_{Con}} \quad \text{eqA1.5}$$

$$729$$

$$730$$

731 Inverting eqA1.5 and dividing by L_{Con} and k_{Con} yields a measure of the total conduit
 732 vessel resistance per unit length (R'_{Con}).

$$733$$

$$734 \quad \frac{\sum R_{Con}}{L_{Con} k_{Con}} = \frac{1}{r_{Con}^4 n_{Con}} = R'_{Con} \quad \text{eqA1.6}$$

$$735$$

$$736$$

737 $1/r_{Con}^4 n_{Con}$ was used to estimate a correlate of vascular resistance per unit length of all
 738 conduit vessels in parallel (R'_{Con}). Similarly, 1st order efferents were assessed using
 739 $1/r_{E1}^4 n_{E1}$. (R'_{E1}). Correlates of afferent and efferent arteriole resistance per unit length
 740 (R'_{AA} , R'_{EA}) were estimated with $1/r_{AA}^4$ and $1/r_{EA}^4$.

741

742 **Appendix 2.**

743

744 **Vascular wall stress**

745 The conduit vessel wall morphology appears similar to filtration capillaries
 746 however, conduits are much wider. Greater diameter tubes or vessels of the same wall
 747 thickness are more susceptible to pressure damage or rupture. How might conduit vessel
 748 wall stress compare with other glomerular vessels?

749

750 **VC and conduit vessel wall stress**

751 The effective wall strength and compliance of systemic capillaries is largely due
 752 to basement membrane/basal lamina (40). Assuming that glomerular vascular wall
 753 strength is due to the glomerular basement membrane (GBM, $0.3\mu\text{m}$ and less than $1/10^{\text{th}}$
 754 of vessel radius) then the Laplace equation (60) can be used to derive the hoop stress (S_h)
 755 of the vascular wall (the force exerted circumferentially trying to pull the wall apart).
 756 For cylindrical conduit vessels:

757

$$758 \quad S_{hCon} = \frac{\Delta P_{Con} r_{Con}}{t_{Con}} \quad \text{eq.A2.1}$$

$$759$$

$$760$$

761 Where ΔP_{Con} is the hydrostatic pressure difference across conduit vessel wall of
 762 radius r_{Con} , and effective wall thickness t_{Con} .

763 The equation for a near spherical VC is half that of an equivalent diameter cylinder:

764

$$S_{hVC} = \frac{\Delta P_{VC} r_{VC}}{2 t_{VC}} \quad \text{eq.A2.2}$$

766

767
 768 *Where ΔP_{VC} is the hydrostatic pressure difference across the VC wall of radius*
 769 *r_{VC} , and effective wall thickness t_{VC} . The effective strength of the arteriolar wall will be*
 770 *a composite of strengths of this thick multilayered structure, however, the arteriole*
 771 *smooth muscle wall thins as it transitions into the VC with only endothelium, basal*
 772 *lamina and collagen sheath surrounded by mesangial matrix.*

773

774 **Parameters used in Calculations**

775 **S_{hAVC} for afferent VC (AVC):**

776 $r_{AVC} = 22\mu\text{m}$ [mean of r'_{AVC} , r''_{AVC} , r'''_{AVC} ; Tab.1],

777 $t_{AVC} = 0.5\text{-}4\mu\text{m}$ [between the first mesangial lamina thickness $\sim 0.5\mu\text{m}$ (see
 778 Fig.8d) and the collagen sheath dispersed over $4\mu\text{m}$ (Tab.4, Fig.8)]

779 $\Delta P_{AVC} = 23\text{mmHg}$ [AVC luminal pressure of 63mmHg (43) minus mesangial
 780 pressure - a high proportion of capillary hydrostatic pressure (9) - likely 40mmHg since
 781 mesangial cells respond to 40mmHg and above (19, 30).]

782

783 $S_{hAVC} = 8 - 66 \text{ kPa}$ (equation A2.2) [$\leq 8 \text{ kPa}$ if the effective ΔP_{AVC} is lower due to
 784 pressure dissipating gradients and effective t_{AVC} thicker due to additional mesangial
 785 matrix support (7)]

786

787 **S_{hMC} for mesangial conduit vessel (MC):**

788 *The mesangial backed conduit vessels (Fig.3a, Mes.Con) adjacent to AVCs would*
 789 *share the same mesangial protection and possibly collagen sheath as the AVCs.*

790 $r_{MC} = 8\mu\text{m}$ [Tab.1]

791 $t_{MC} = 0.5\mu\text{m}$ to $4\mu\text{m}$ [Tab.4, Fig.8]

792 $\Delta P_{MC} = 23\text{mmHg}$ [see above]

793

794 $S_{hMC} = 6 - 48 \text{ kPa}$ (equation A2.1) [$\leq 6 \text{ kPa}$, S_{hAVC} caveat as above]

795

796 **S_{hGC} for glomerular filtration barrier conduit vessel (GC):**

797 *The conduit vessels away from the AVC are connected to mesangium only on a*
 798 *small part of their circumference the rest being normal GFB and GBM (Fig.3a, GFB*
 799 *Con)*

800 $r_{GC} = 8\mu\text{m}$ [Tab.1]

801 $t_{GC} = 0.3\mu\text{m}$ [GBM thickness]

802 $\Delta P_{GC} = 38\text{mmHg}$ [luminal P (63mmHg) minus urinary space P (25mmHg)]

803

804 $S_{hGC} = 133 \text{ kPa}$ (equation A2.1)

805

806 **S_{hFC} for filtration capillaries (FC):**

807 $r_{FC} = 3.5\mu\text{m}$

808 $t_{FC} = 0.3\mu\text{m}$ [GBM thickness]

809 $\Delta P_{FC} = 38\text{mmHg}$ [luminal P (63mmHg) minus urinary space P (25mmHg)]

810
811
812

$$S_{hFC} = 58 \text{ kPa (equation A2.1)}$$

	Subscript abbreviation	ΔP	r	t	S_h
		(mmHg)	(μm)	(μm)	(kPa)
Afferent VC	AVC	23	22	0.5-4.0	$\leq 8-66$
Mesangial conduit	MC	23	8	0.5-4.0	$\leq 6-48$
GFB conduit	GC	38	8	0.3	133 *
Filtration Caps.	FC	38	3.5	0.3	58

813 **Table A1.** Calculated vascular hoop stress S_h . The peak is in the GFB conduit vessels (*).
814

815

816 S_h is difficult to estimate in the mesangial backed AVC and mesangial conduit
817 vessels but our maximum estimate is less than half the value for the GFB Conduit. S_h falls
818 in the filtration capillaries of the same wall thickness but these are protected by their
819 small radius. At the efferent end the reduced radii and complete mesangial encasement of
820 VC and of the short EI vessels would result in lower S_h of the equivalent efferent vessels
(not shown).

821 In conclusion, in human glomeruli, GFB conduit walls (GC) mark a peak of hoop
822 stress caused by the relatively thin wall for the large diameter. While the AVC and the
823 early conduit vessel are protected by mesangial backing, any mesangial disruption
824 through immune-mediated damage, cell invasion or proliferation or disruption to the
825 collagen sheath will change S_{hAVC} and S_{hMC} making AVC and mesangial conduit vessels
826 vulnerable to pressure changes.

827

828 Acknowledgements

829 This study was financed by The Richard Bright Research Trust until 2014 and
830 then by Kidney Research UK (2014-2015). Early parts of this study have been presented
831 to the British Microcirculation Society annual meetings 2011, 2012 and 2013, 2014, 2015
832 and to ASN kidney week 2012. We would like to thank W. Brewer, J. Stewer, P. Gurney,
833 P. Davy, D. Widden, H. Hawke, T. Cobleigh and all for their help.

834

835 REFERENCES

- 836 1. **Arendshorst WJ and Gottschalk CW.** Glomerular ultrafiltration dynamics:
837 historical perspective. *Am J Physiol* 248: F163-174, 1985.
- 838 2. **Arkill KP, Moger J, and Winlove CP.** The structure and mechanical properties
839 of collecting lymphatic vessels: an investigation using multimodal nonlinear microscopy.
840 *J Anat* 216: 547-555, 2010.
- 841 3. **Batchelor GK.** *An Introduction to fluid dynamics:* Cambridge University Press,
842 2000.
- 843 4. **Bohle A, Aeikens B, Eenboom A, Fronholt L, Plate WR, Xiao JC,**
844 **Greschniok A, and Wehrmann M.** Human glomerular structure under normal
845 conditions and in isolated glomerular disease. *Kidney Int Suppl* 67: S186-188, 1998.
- 846 5. **Bowman W.** On the structure and use of the malpighian bodies of the kidney,
847 with observations on the circulation through that gland. *Phil Trans R Soc Lond* 132: 57-
848 80, 1842.

- 849 6. **Boyer CC.** The vascular pattern of the renal glomerulus as revealed by plastic
850 reconstruction from serial sections. *Anat Rec* 125: 433-441, 1956.
- 851 7. **Cohen AH.** Collagen Type III Glomerulopathies. *Advances in chronic kidney*
852 *disease* 19: 101-106, 2012.
- 853 8. **Darmady EM, Offer J, and Woodhouse MA.** The parameters of the ageing
854 kidney. *J Pathol* 109: 195-207, 1973.
- 855 9. **Elger M, Sakai T, and Kriz W.** The vascular pole of the renal glomerulus of rat.
856 *Adv Anat Embryol Cell Biol* 139: 1-98, 1998.
- 857 10. **Ellis EN, Mauer SM, Sutherland DE, and Steffes MW.** Glomerular capillary
858 morphology in normal humans. *Lab Invest* 60: 231-236, 1989.
- 859 11. **Evan AP, Jr., Stoeckel JA, Loemker V, and Baker JT.** Development of the
860 intrarenal vascular system of the puppy kidney. *Anat Rec* 194: 187-199, 1979.
- 861 12. **Feng MG and Navar LG.** Afferent arteriolar vasodilator effect of adenosine
862 predominantly involves adenosine A2B receptor activation. *Am J Physiol Renal Physiol*
863 299: F310-315, 2010.
- 864 13. **Fleischmajer R, Jacobs L, 2nd, Perlish JS, Katchen B, Schwartz E, and**
865 **Timpl R.** Immunochemical analysis of human kidney reticulin. *The American journal of*
866 *pathology* 140: 1225-1235, 1992.
- 867 14. **Gubler MC, Dommergues JP, Foulard M, Bensman A, Leroy JP, Broyer M,**
868 **and Habib R.** Collagen type III glomerulopathy: a new type of hereditary nephropathy.
869 *Pediatric nephrology* 7: 354-360, 1993.
- 870 15. **Hall TJ, Insana MF, Harrison LA, and Cox GG.** Ultrasonic measurement of
871 glomerular diameters in normal adult humans. *Ultrasound Med Biol* 22: 987-997, 1996.
- 872 16. **Harrison-Bernard LM, Monjure CJ, and Bivona BJ.** Efferent arterioles
873 exclusively express the subtype 1A angiotensin receptor: functional insights from genetic
874 mouse models. *Am J Physiol Renal Physiol* 290: F1177-1186, 2006.
- 875 17. **Herbert SC, Reilly, R.F., Kriz, W.** Structural functional relationships in the
876 kidney. In: *Diseases of the Kidney and Urinary Tract* (7th ed.), edited by Schrier RW.
877 Philadelphia: Lippincott Williams & Wilkins, 2001, p. 3-57.
- 878 18. **Hill GS, Heudes D, Jacquot C, Gauthier E, and Bariety J.** Morphometric
879 evidence for impairment of renal autoregulation in advanced essential hypertension.
880 *Kidney Int* 69: 823-831, 2006.
- 881 19. **Hishikawa K, Oemar BS, and Nakaki T.** Static pressure regulates connective
882 tissue growth factor expression in human mesangial cells. *The Journal of biological*
883 *chemistry* 276: 16797-16803, 2001.
- 884 20. **John R and Herzenberg AM.** Renal toxicity of therapeutic drugs. *J Clin Pathol*
885 62: 505-515, 2009.
- 886 21. **Johnston WB.** A reconstruction of a glomerulus of the human kidney.
887 *Anatomischer Anzeiger* 16: 260-266, 1899.
- 888 22. **Kanwar YS, Venkatachalam, M.A.** Ultrastructure of glomerulus and
889 juxtaglomerular apparatus. In: *Handbook of Physiology*, edited by Windhager EE. New
890 York: Oxford University Press, 1992, p. 3-40.
- 891 23. **Kessler LW, Fields SI, and Dunn F.** Acoustic microscopy of mammalian
892 kidney. *J Clin Ultrasound* 2: 317-320, 1974.
- 893 24. **Kimura K, Tojo A, Matsuoka H, and Sugimoto T.** Renal arteriolar diameters in
894 spontaneously hypertensive rats. Vascular cast study. *Hypertension* 18: 101-110, 1991.

- 895 25. **Kriz W, Hackenthal E, Nobiling R, Sakai T, Elger M, and Hahnel B.** A role
896 for podocytes to counteract capillary wall distension. *Kidney Int* 45: 369-376, 1994.
- 897 26. **Kriz W, Hosser H, Hahnel B, Simons JL, and Provoost AP.** Development of
898 vascular pole-associated glomerulosclerosis in the Fawn-hooded rat. *J Am Soc Nephrol* 9:
899 381-396, 1998.
- 900 27. **Kriz W, Mundel P, and Elger M.** The contractile apparatus of podocytes is
901 arranged to counteract GBM expansion. *Contrib Nephrol* 107: 1-9, 1994.
- 902 28. **Lai EY, Onozato ML, Solis G, Aslam S, Welch WJ, and Wilcox CS.**
903 Myogenic responses of mouse isolated perfused renal afferent arterioles: effects of salt
904 intake and reduced renal mass. *Hypertension* 55: 983-989, 2010.
- 905 29. **Lu Y, Fu Y, Ge Y, Juncos LA, Reckelhoff JF, and Liu R.** The vasodilatory
906 effect of testosterone on renal afferent arterioles. *Gen Med* 9: 103-111, 2012.
- 907 30. **Mattana J and Singhal PC.** Applied pressure modulates mesangial cell
908 proliferation and matrix synthesis. *Am J Hypertens* 8: 1112-1120, 1995.
- 909 31. **McLachlan MS, Guthrie JC, Anderson CK, and Fulker MJ.** Vascular and
910 glomerular changes in the ageing kidney. *J Pathol* 121: 65-78, 1977.
- 911 32. **McMillan DE.** The microcirculation in diabetes. *Microcirc Endothelium*
912 *Lymphatics* 1: 3-24, 1984.
- 913 33. **Min W and Yamanaka N.** Three-dimensional analysis of increased vasculature
914 around the glomerular vascular pole in diabetic nephropathy. *Virchows Arch A Pathol*
915 *Anat Histopathol* 423: 201-207, 1993.
- 916 34. **Moore L, Williams R, and Staples A.** Glomerular dimensions in children under
917 16 years of age. *J Pathol* 171: 145-150, 1993.
- 918 35. **Morita T and Churg J.** Mesangiolytic. *Kidney Int* 24: 1-9, 1983.
- 919 36. **Murray CD.** The Physiological Principle of Minimum Work: I. The Vascular
920 System and the Cost of Blood Volume. *Proc Natl Acad Sci U S A* 12: 207-214, 1926.
- 921 37. **Murray CD.** The Physiological Principle of Minimum Work: II. Oxygen
922 Exchange in Capillaries. *Proc Natl Acad Sci U S A* 12: 299-304, 1926.
- 923 38. **Navar LG, Evan AP, and Rosivall L.** Microcirculation of the kidneys. In: *The*
924 *Physiology and Pharmacology of the Microcirculation*, edited by Mortillaro NA:
925 Academic press, 1983, p. 397-488.
- 926 39. **Neal CR, Crook H, Bell E, Harper SJ, and Bates DO.** Three-dimensional
927 reconstruction of glomeruli by electron microscopy reveals a distinct restrictive urinary
928 subpodocyte space. *J Am Soc Nephrol* 16: 1223-1235, 2005.
- 929 40. **Neal CR and Michel CC.** Effects of temperature on the wall strength and
930 compliance of frog mesenteric microvessels. *J Physiol* 526 Pt 3: 613-622, 2000.
- 931 41. **Neal CR, Muston PR, Njegovan D, Verrill R, Harper SJ, Deen WM, and**
932 **Bates DO.** Glomerular filtration into the subpodocyte space is highly restricted under
933 physiological perfusion conditions. *Am J Physiol Renal Physiol* 293: F1787-1798, 2007.
- 934 42. **Nordsletten DA, Blackett S, Bentley MD, Ritman EL, and Smith NP.**
935 Structural morphology of renal vasculature. *Am J Physiol Heart Circ Physiol* 291: H296-
936 309, 2006.
- 937 43. **Oken DE.** An analysis of glomerular dynamics in rat, dog, and man. *Kidney Int*
938 22: 136-145, 1982.

- 939 44. **Osterby R, Bangstad HJ, and Rudberg S.** Follow-up study of glomerular
940 dimensions and cortical interstitium in microalbuminuric type 1 diabetic patients with or
941 without antihypertensive treatment. *Nephrol Dial Transplant* 15: 1609-1616, 2000.
- 942 45. **Osterby R, Hartmann A, and Bangstad HJ.** Structural changes in renal
943 arterioles in Type I diabetic patients. *Diabetologia* 45: 542-549, 2002.
- 944 46. **Painter PR, Eden P, and Bengtsson HU.** Pulsatile blood flow, shear force,
945 energy dissipation and Murray's Law. *Theor Biol Med Model* 3: 31, 2006.
- 946 47. **Preston K, Jr., Joe B, Siderits R, and Welling J.** Three-dimensional
947 reconstruction of the human renal glomerulus. *J Microsc* 177: 7-17, 1995.
- 948 48. **Remuzzi A, Brenner BM, Pata V, Tebaldi G, Mariano R, Belloro A, and**
949 **Remuzzi G.** Three-dimensional reconstructed glomerular capillary network: blood flow
950 distribution and local filtration. *Am J Physiol* 263: F562-572, 1992.
- 951 49. **Rowe M.** Measurements and computations of flow in pipe bends. *J Fluid Mech*
952 43: 771-783, 1970.
- 953 50. **Salmon AH, Toma I, Sipos A, Muston PR, Harper SJ, Bates DO, Neal CR,**
954 **and Peti-Peterdi J.** Evidence for restriction of fluid and solute movement across the
955 glomerular capillary wall by the subpodocyte space. *Am J Physiol Renal Physiol* 293:
956 F1777-1786, 2007.
- 957 51. **Samuel T, Hoy WE, Douglas-Denton R, Hughson MD, and Bertram JF.**
958 Determinants of glomerular volume in different cortical zones of the human kidney. *J Am*
959 *Soc Nephrol* 16: 3102-3109, 2005.
- 960 52. **Sato Y, Hara S, Fujimoto S, Yamada K, Sakamaki H, and Eto T.** Minimal
961 change nephrotic syndrome after allogenic hematopoietic stem cell transplantation. *Intern*
962 *Med* 43: 512-515, 2004.
- 963 53. **Shimizu H, Shinohara N, and Yokoyama T.** Topological analysis of the three-
964 dimensional structure of the human renal glomerulus using a computer-aided
965 reconstruction system. *Microvasc Res* 36: 130-139, 1988.
- 966 54. **Skov K, Mulvany MJ, and Korsgaard N.** Morphology of renal afferent
967 arterioles in spontaneously hypertensive rats. *Hypertension* 20: 821-827, 1992.
- 968 55. **Sorensen FH.** Quantitative studies of the renal corpuscles. I. Intraglomerular,
969 interglomerular and interfocal variation in the normal kidney. *Acta Pathol Microbiol*
970 *Scand A* 80: 115-124, 1972.
- 971 56. **Stout LC and Whorton EB.** Pathogenesis of extra efferent vessel development
972 in diabetic glomeruli. *Hum Pathol* 38: 1167-1177, 2007.
- 973 57. **Troncoso Brindeiro CM, Lane PH, and Carmines PK.** Tempol prevents
974 altered K(+) channel regulation of afferent arteriolar tone in diabetic rat kidney.
975 *Hypertension* 59: 657-664, 2012.
- 976 58. **Venkatachalam MA, Kriz, W.** Anatomy. In: *Heptinstall's Pathology of the*
977 *Kidney* (5th ed.), edited by Jennette JC, Olson, J.L., Schwartz, M.M., Silva, F.G.
978 Philadelphia: Lippincott Raven, 1998, p. 3-66.
- 979 59. **West JB.** *Respiratory Physiology - The Essentials*. Baltimore: Williams and
980 Wilkins 1979.
- 981 60. **Westerhof N, Stergiopoulos, N, Noble, MIM.** *Snapshot on Hemodynamics: An*
982 *Aid for Clinical Research and Graduate Education*: Springer Verlag, 2010.

983 61. **Willassen Y and Ofstad J.** Postglomerular vascular hydrostatic and oncotic
984 pressures during acute saline volume expansion in normotensive man. *Scand J Clin Lab*
985 *Invest* 39: 707-715, 1979.

986
987

988 **Figure 1. Afferent arteriole and glomerulus connectivity.** Selected light micrographs
989 from a 1 μ m serial section stack to show the connectivity of an afferent arteriole (25 μ m
990 diameter) with a small artery (110 μ m diameter interlobular or feed artery). Identifying
991 the root/route of the vessels entering the glomerulus allows identification of afferent and
992 efferent arterioles. Notice the afferent arteriole goes through a right angle as it enters the
993 glomerulus. AA – afferent arteriole; GC - glomerular capillary; serial section number at
994 bottom right.

995

996 **Figure 2A&B. Serial resin sections through a glomerulus.** Selected light micrographs
997 from 2 complete 1 μ m serial section series to show the route blood takes from an afferent
998 arteriole (AA) into an afferent vascular chamber (AVC) leading into conduit vessels
999 (Con) of high capacity and few branches. At the other end of the microcirculation many
1000 branching efferent 1st order vessels (E1) drain into a smaller efferent vascular chamber
1001 (EVC) leading to an efferent arteriole (EA). Serial section numbers at bottom left. Scale
1002 bar 100 μ m in micrograph of section 254 or 198 (see Supplemental video S2A and S2B
1003 for glomerular image stacks of Fig.2A and B respectively, Supplemental S2C and S2D
1004 for a reconstruction of afferent and efferent parts of Fig.2B)

1005

1006 **Figure 3. Scale diagram of glomerular vasculature; the smallest vascular chambers.**
1007 **A/** Scale diagram of the Afferent (light grey) and Efferent (white) ends of the glomerular
1008 vasculature. Diagram shows size and branch relationships between arterioles, VCs and
1009 1st order vessels (mesangium close to vascular pole - dark grey) (diameters from tab.
1010 1&2). To illustrate VC volume in relation to attached vessels the length of attached
1011 vessels accommodating VC volume has been shown - AVC volume would distribute
1012 along 112 μ m length (delimited by hoops x, y) of afferent arteriole (AA) or distribute
1013 along 31 μ m length (delimited by hoops x', y') of 7 conduit vessels (Con; 3 of 7 shown).
1014 The EVC volume would fill 138 μ m length of efferent arteriole (EA; hoops p, q) or 28 μ m
1015 length of 13 1st order vessels (E1; hoops p', q' , 4 of 13 shown). Scale bar 100 μ m. A2
1016 and E2 – second order vessel examples. Mes.Con - Conduit vessel embedded in
1017 mesangium. GFB.Con - Conduit vessel with GFB surface and minor mesangial
1018 attachment. **B/** Minimal Vascular Chambers. The upper diagram shows VC as in our
1019 reconstructions but both V_{AVC} and V_{EVC} decrease as V_G decreases (Fig.4c&d). VC
1020 shrinkage in the radial direction would reduce the diameter and VC volume until it was a
1021 continuation of the attached arteriole (Fig.4 C&D).

1022

1023 **Figure 4. Conduit branching and diameter; VC volume scales with glomerular**
1024 **volume.** **A/** Histogram of branch separation between 2nd order branches (A2 or E2)
1025 emerging from 1st order vessels (Con or E1). Branch intervals were assessed in 9
1026 glomeruli, conduit vessels (Con, filled bars) are longer and less branched than 1st order
1027 efferent vessels (E1, open bars) (Mann Whitney U test medians (32.8, 15 μ m),
1028 $P < 0.0001$). **B/** Histogram of 1st order vessel diameter coming off Vascular Chambers.

1029 Conduit vessels (filled bars) are significantly wider than Efferent first order vessels (open
1030 bars), efferent distribution is skewed towards lower values (15.3(12.8-18.9) v. 9.0(7.0-
1031 11.1); median(IQR); Mann Whitney U test, $p < 0.0001$). **C/** Afferent VC volume and **D/**
1032 Efferent VC volume scale with glomerular volume to a highly significant level ($R^2 =$
1033 0.517 $P=0.004$; $R^2 = 0.419$ $P=0.012$ respectively). A minimum possible V_{AVC} and V_{EVC}
1034 (See Fig.3B) is also plotted to show V_G where VCs are a continuation of the attached
1035 arteriole (i.e. no VC widening).
1036

1037 **Figure 5. Conduit diameter changes with mesangium; conduit podocyte attachment;**
1038 **resistance v capacity examples** **A/** Conduit diameter changes relative to mesangial
1039 cover. Conduit vessel diameters adjacent to the afferent VC with mesangial cover of 80-
1040 100% (GFB coverage 0-20%) were compared with diameters of low mesangial covered
1041 (distal) regions of the same vessel. The fold change in diameter shows a significant
1042 diameter increase of 7.4% (*) when mesangial cover is minimal (0-14% i.e. GFB 86-
1043 100%). Paired t-tests and Wilcoxon matched pair test ($P=0.04$). **B/** Histogram of
1044 podocyte cell body (PCB) area coverage of the filtration barrier of conduit vessels (filled
1045 bars) and small filtration capillaries (open bars). Conduits have significantly less PCB
1046 coverage of the GFB than filtration capillaries (ttest - $P < 0.0001$). **C/** Conduit resistance
1047 versus Afferent VC volume. A significant negative correlation exists between a correlate
1048 of conduit resistance (R'_{Con}) and afferent VC volume (V_{AVC}) ($R^2 = 0.327$, $P=0.033$). **D/**
1049 Efferent arteriole resistance per unit length (R'_{EA}) reduces in line with increasing V_G (R^2
1050 $= 0.47$, $P=0.007$).
1051
1052

1053 **Figure 6. Vascular widenings in single sections. Murray constant from vascular**
1054 **radii** **A/** Observed occurrence of glomerular vascular widening in single sections. The
1055 frequency with which widening (implying VC presence) was observed at vascular poles
1056 in immersion and perfusion fixed glomeruli. SC - subcapsular glomeruli; JM - juxta-
1057 medullary glomeruli; JMSC - JM and SC glomeruli combined. (n = number of kidneys)
1058 **B/** In 14 glomeruli a Murray constant ($K = r^3 n_V$; where r is radius, n_V is vessel number;
1059 see text) was calculated for the afferent and efferent arteriolar tree leading through the
1060 VCs and thence into the 1st order vessels (Con and E1). In 2 glomeruli K was calculated
1061 for 2nd order vessels. The Murray relationship of equal K at each vessel level is absent in
1062 the AVC, EVC and conduit vessels.
1063

1064 **Figure 7. Multiphoton imaging of glomeruli.** Images obtained by combining two
1065 photon fluorescence (TPF) signal images with second harmonic generation (SHG) images
1066 of an unfixed human glomerulus. The capillary walls emit a TPF signal (green) with most
1067 of the smaller filtration capillaries showing collapse. A banded Collagen signal (SHG
1068 blue) is located adjacent to a VC wall (intense Bowman's capsule Collagen has been
1069 blanked). Section s1 is close to the tissues physical surface; A - arteriole, (optical section
1070 $1\mu\text{m}$ deep). S31 shows a wide incomplete region of banded collagen around an
1071 uncollapsed region (VC) connected with A in s1. The banded collagen region has
1072 disappeared in s37 but offshoots in attached vessels appear in s37 (right of VC) and s52
1073 (left of VC position). Diameter of field - $200\mu\text{m}$. (See supplemental video S3 for full
1074 section series)

1075

1076

1077 **Figure 8. Transmission electron micrographs of Vascular chamber walls.** Vascular
1078 Chamber were imaged using a Tecnai 12 electron microscope, low power (A) shows a
1079 vascular pole an AVC, conduit vessels (Con) and urinary space (US). (B) Montage of
1080 micrographs to show the disposition of the banded collagen fibres around the VC walls.
1081 White dotted lines show the extent of the mesangial matrix where banded collagen fibres
1082 were evident. (C) Area C from montage B with matrix rich in banded collagen (BCM)
1083 and where collagen is absent (M). (D) Area D from montage B with banded collagen
1084 fibres.

1085

1086 **Table 1 & 2. Afferent and efferent vascular diameters.** Diameters of afferent and
1087 efferent vessels from resin embedded glomeruli (14) from 4 human kidneys. In all cases
1088 the afferent and efferent arterioles widen to form ellipsoidal chambers with between 2
1089 and 11 high capacity conduit vessels emerging and conveying fluid away to the filtration
1090 capillaries. Blood from the filtration capillaries converges into 3 to 22 narrow efferent
1091 first order vessels which converge into the Efferent VC and thence the efferent arteriole.
1092 [In the 14 glomeruli analysed, 2 extra wide conduit vessels (19-24 μ m) were found, 1
1093 extrawide E1 drainage vessel (20-27 μ m) but the branching was frequent as in other E1
1094 vessels]. Vascular chamber dimensions: min.diam.; minimum diameter measured in the
1095 section plane avoiding oblique vessel sections. max.diam.; maximum diameter measured
1096 in the section plane avoiding oblique vessel sections. Secn. depth diam; diameter
1097 measured in the sectioning direction. sem; standard error of the mean

1098

1099 **Table 3. Vascular resistance and capacity relationships.** Significant correlations
1100 (8 out of 21) between 7 variables measured in human glomerular initial vasculature.
1101 Correlates of vascular resistance for afferent arterioles (R_{AA}), Conduit vessels (R_{Con}), first
1102 order efferent vessels (R_{E1}) and efferent arterioles (R_{EA}) were compared with each other
1103 and with AVC volume (V_{AVC}) glomerular volume (V_G) and EVC volume (V_{EVC}). +
1104 positive correlation, - negative correlation; * = $P < 0.05$, ** = $P \leq 0.01$; **** = $P \leq$
1105 0.0001; § higher significance with outlier removed.

1106

1107

1108 **Table 4. Vascular diameters and wall thicknesses - all experiments.** Comparison of
1109 AA, AVC, Conduit, E1, EVC, and EA measurements from resin section reconstruction
1110 with the same features in fixed and fresh glomeruli reconstructed from confocal and
1111 multiphoton microscope z stacks (SHG and TPF). EVC and AVC values have been
1112 averaged together for all 3 axes. AVC Collagen sheath (AVC Coll) enshrouded AVC and
1113 some parts of conduit vessels but scant evidence in EVC or E1 (multiphoton microscopy
1114 only). G and K indicate numbers of glomeruli and kidneys used. * not all quantities were
1115 observable and measureable.

1116

1117 **Supplemental**

1118 ***Supplemental video legends***

1119

1120 *Fig. S2a. Image stack for Fig 2a glomerulus.*

1121 *Video to show the full image stack formed by Image J software from original 1 μ m*
1122 *serial section images. Stills in Fig.2a. Field of view 170 x 200 μ m approximately.*
1123
1124 *Fig.S2b, Image stack for Fig 2b glomerulus.*
1125 *Video to show the full image stack formed by Image J software from original 1 μ m*
1126 *serial section images. Stills in Fig.2b. Field of view 190 x 220 μ m approximately.*
1127
1128 *Fig. S2c. Reconstruction x derived from Fig. S2b.*
1129 *Red afferent arteriole derived vessels meeting with blue efferent arteriole derived*
1130 *vessels at purple points. Rotation around x axis. Not all vessels shown. Scale marks in*
1131 *μ m.*
1132
1133 *Fig. S2d. Reconstruction y derived from Fig. S2b.*
1134 *Red afferent arteriole derived vessels meeting with blue efferent arteriole derived*
1135 *vessels at purple points. Rotation around y axis. Not all vessels shown. Scale marks in*
1136 *μ m.*
1137
1138 *Fig. S3. Reconstruction of an unfixed glomerulus from multiphoton microscope images.*
1139 *TPF and SHG modes were used to image the vessel walls (green) and banded collagen*
1140 *(blue) respectively. The intense blue signal from the collagen of Bowman's capsule was*
1141 *covered by a circular black mask. The afferent arteriole opens into a VC at the 7*
1142 *o'clock position, the banded collagen signal follows the walls of the VC and into the*
1143 *conduit vessels. Field width 200 μ m*
1144

1145 **Footnote 1**
1146 *[Afferent arteriole conductance estimated from the 4th power of vessel radii (mice, $r = 5-$*
1147 *$6.5\mu\text{m}$, (16, 28, 29); rats, $r = 7-9.5\mu\text{m}$ (12, 24, 54, 57); human, $r = 11\mu\text{m}$ [this article])*
1148 *with human glomerular volume estimated from glomerular diameter (mouse= $70\mu\text{m}$,*
1149 *rat= $120\mu\text{m}$ and human= $200\mu\text{m}$)]*
1150

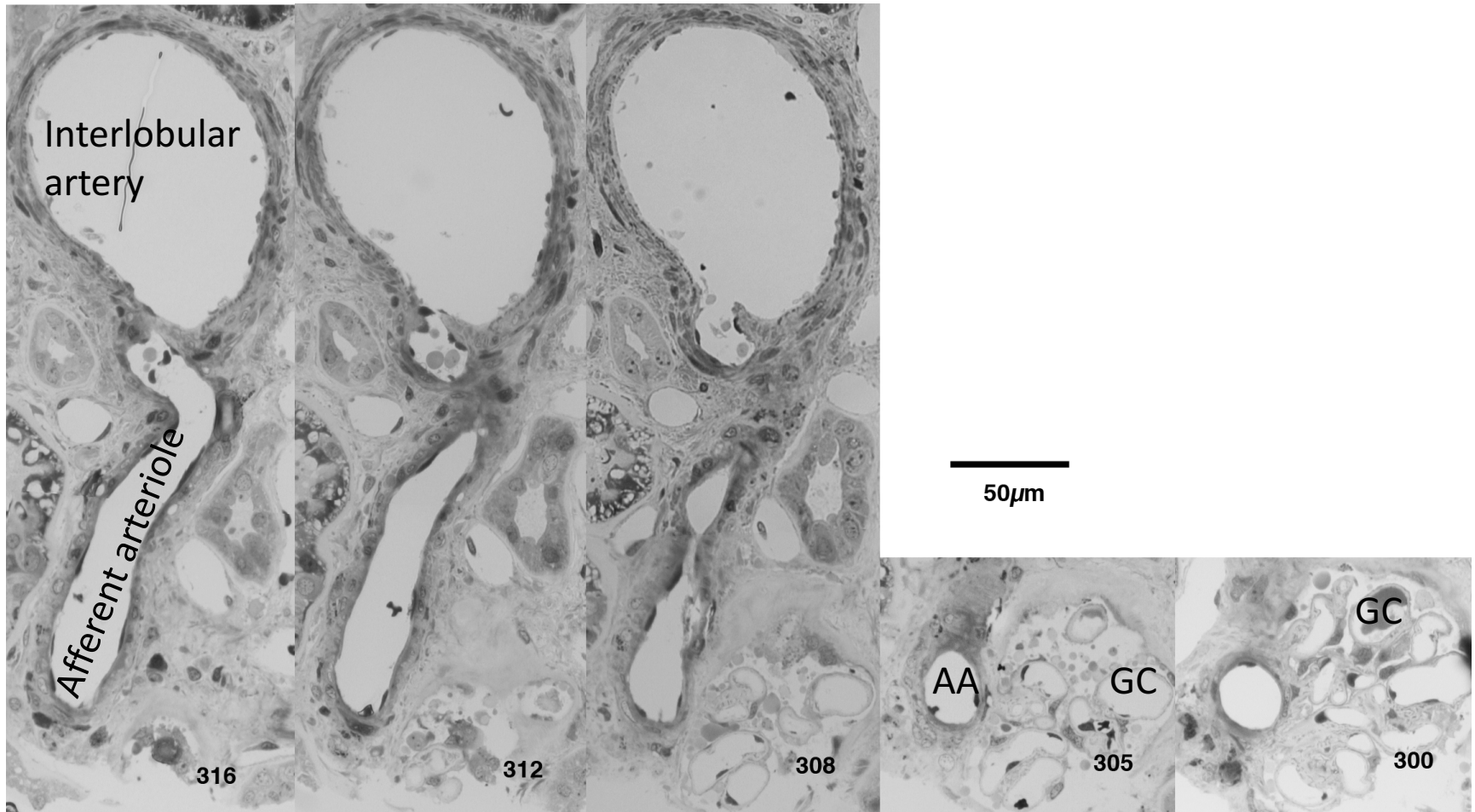


Figure 1. Afferent arteriole and glomerulus connectivity. Selected light micrographs from a 1µm serial section stack to show the connectivity of an afferent arteriole (25µm diameter) with a small artery (110µm diameter interlobular or feed artery). Identifying the root/route of the vessels entering the glomerulus allows identification of afferent and efferent arterioles. Notice the afferent arteriole goes through a right angle as it enters the glomerulus. AA – afferent arteriole; GC - glomerular capillary; serial section number at bottom right.

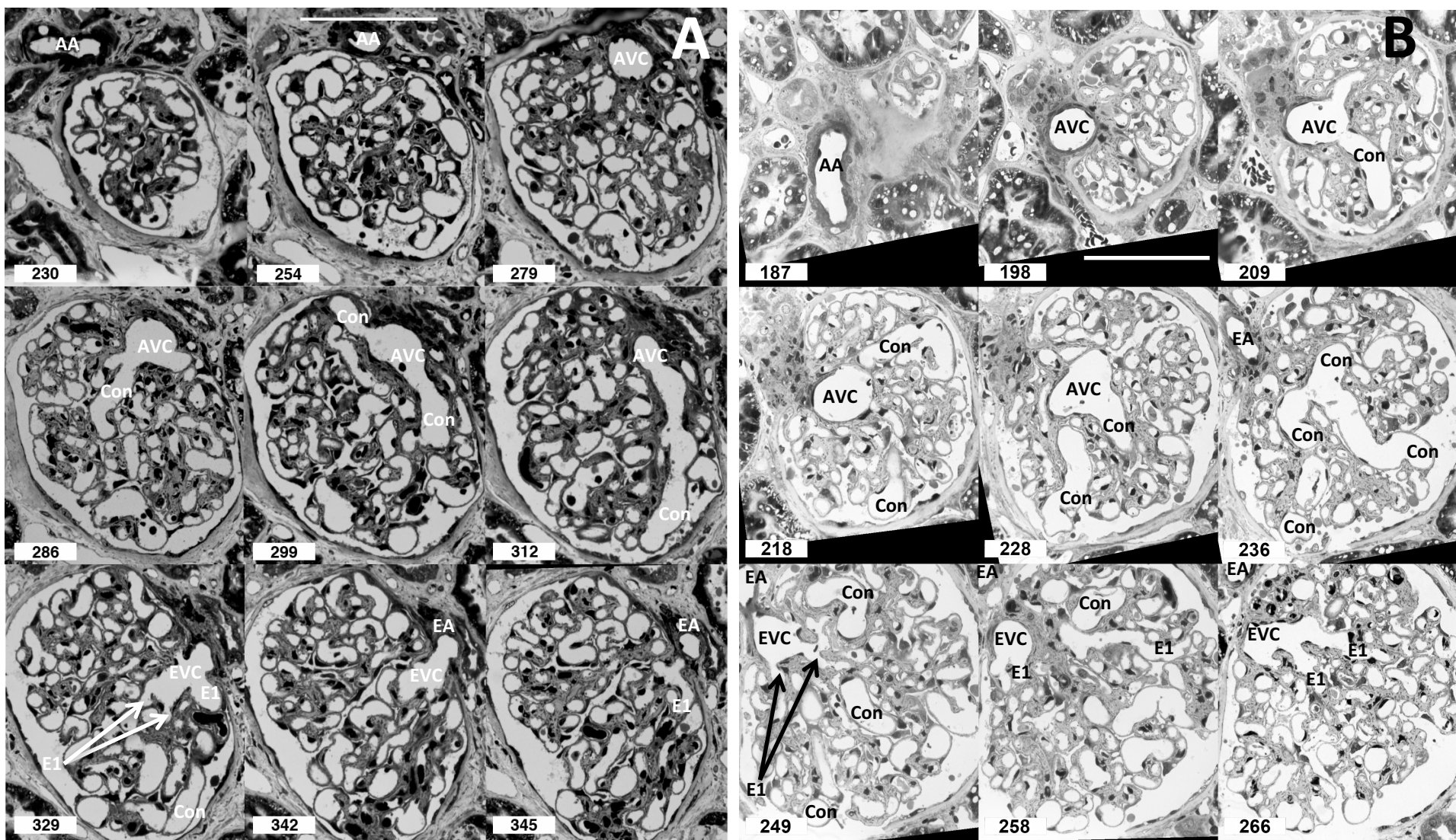


Figure 2A&B. Serial resin sections through a glomerulus. Selected light micrographs from 2 complete 1 μ m serial section series to show the route blood takes from an afferent arteriole (AA) into an afferent vascular chamber (AVC) leading into conduit vessels (Con) of high capacity and few branches. At the other end of the microcirculation many branching efferent 1st order vessels (E1) drain into a smaller efferent vascular chamber (EVC) leading to an efferent arteriole (EA). Serial section numbers at bottom left. Scale bar 100 μ m in micrograph of section 254 or 198 (see Supplemental video S2A and S2B for glomerular image stacks of Fig.2A and B respectively, Supplemental S2C and S2D for a reconstruction of afferent and efferent parts of Fig.2B)

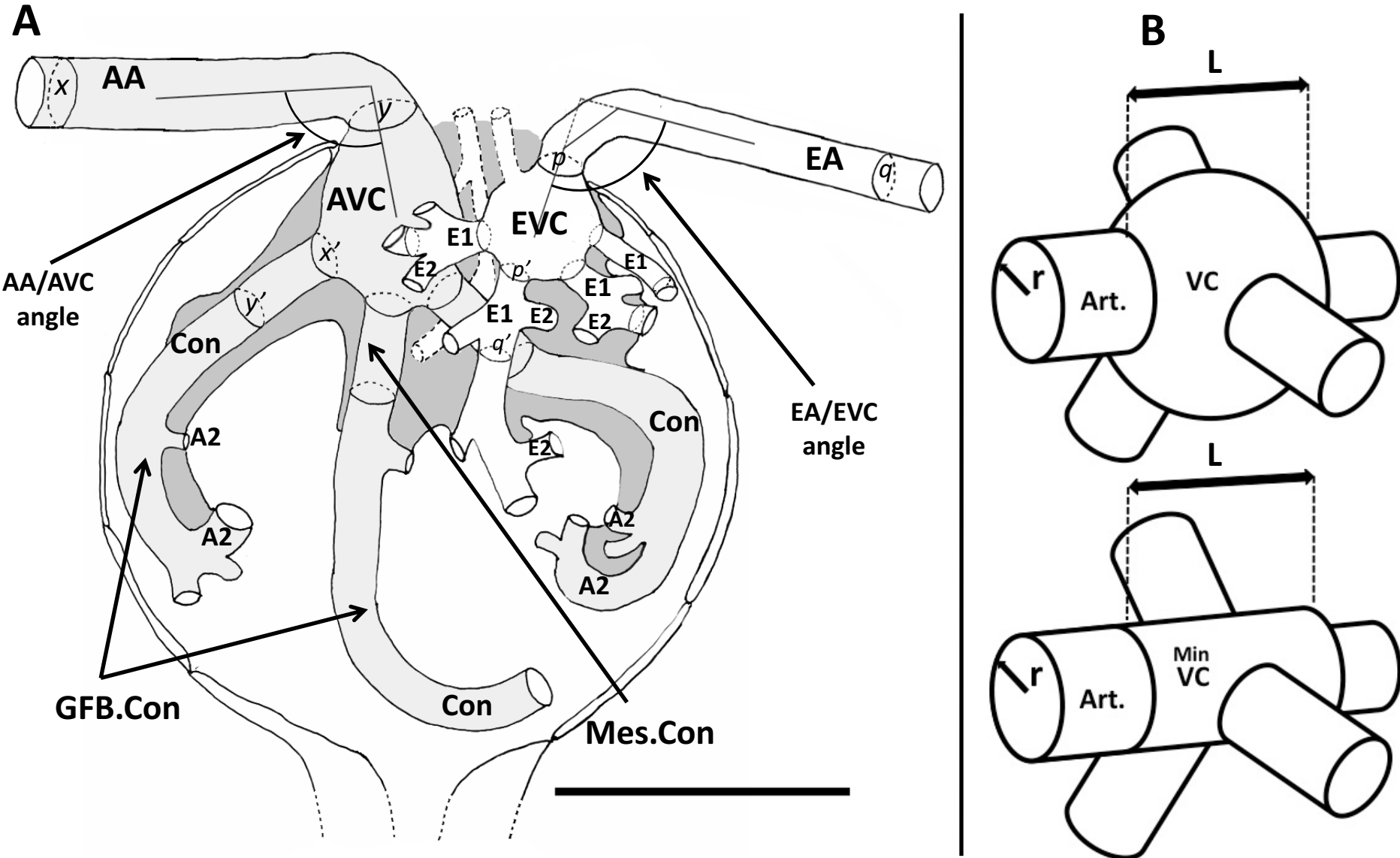


Figure 3. Scale diagram of glomerular vasculature; the smallest vascular chambers. A/ Scale diagram of the Afferent (light grey) and Efferent (white) ends of the glomerular vasculature. Diagram shows size and branch relationships between arterioles, VCs and 1st order vessels (mesangium close to vascular pole - dark grey) (diameters from tab. 1&2). To illustrate VC volume in relation to attached vessels the length of attached vessels accommodating VC volume has been shown - AVC volume would distribute along 112 μ m length (delimited by hoops x, y) of afferent arteriole (AA) or distribute along 31 μ m length (delimited by hoops x', y') of 7 conduit vessels (Con; 3 of 7 shown). The EVC volume would fill 138 μ m length of efferent arteriole (EA; hoops p, q) or 28 μ m length of 13 1st order vessels (E1; hoops p', q', 4 of 13 shown). Scale bar 100 μ m. A2 and E2 - second order vessel examples. Mes.Con - Conduit vessel embedded in mesangium. GFB.Con - Conduit vessel with GFB surface and minor mesangial attachment. **B/** Minimal Vascular Chambers. The upper diagram shows VC as in our reconstructions but both V_{AVC} and V_{EVC} decrease as V_G decreases (Fig.4c&d). VC shrinkage in the radial direction would reduce the diameter and VC volume until it was a continuation of the attached arteriole (Fig.4 C&D).

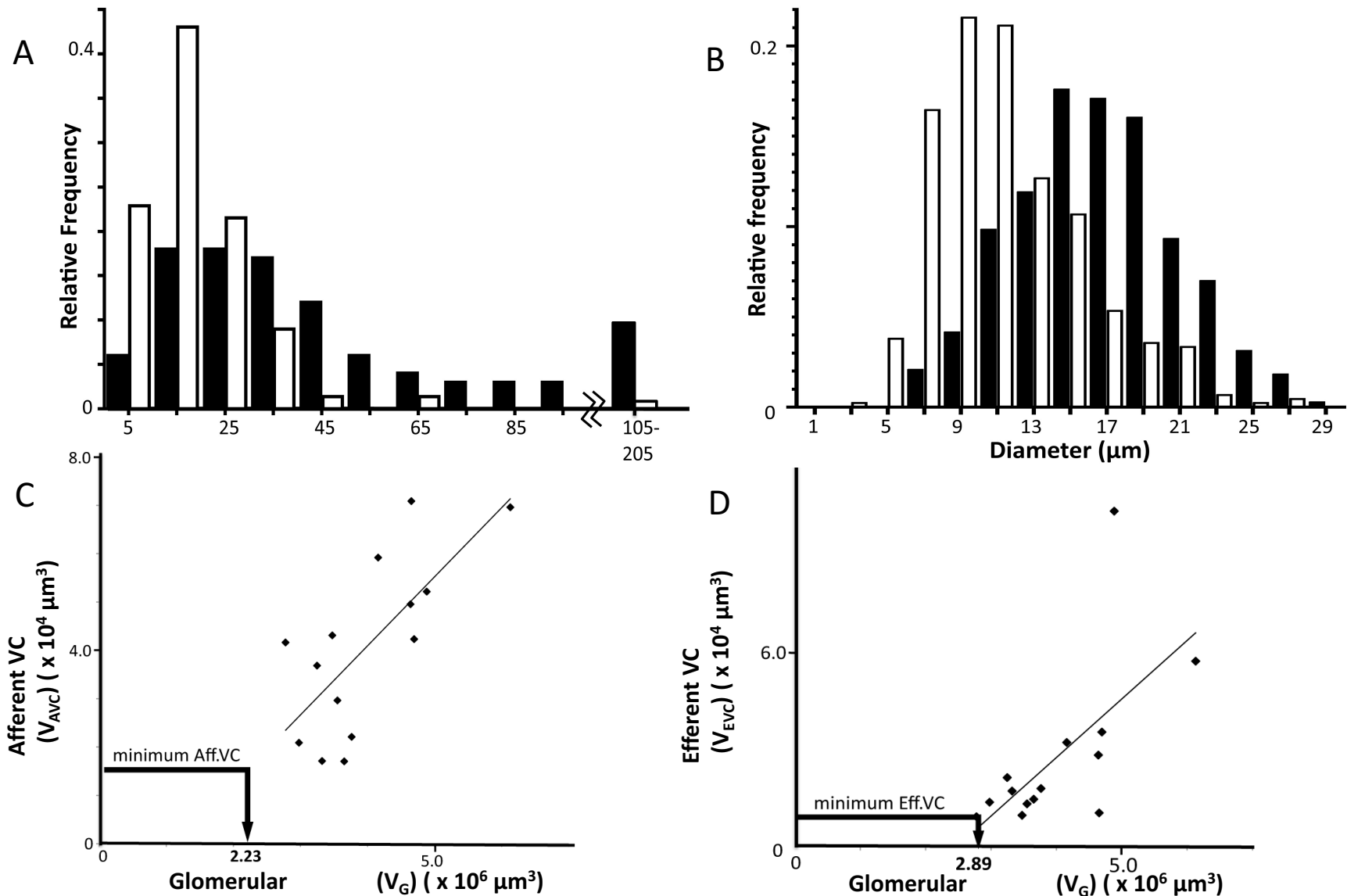


Figure 4. Conduit branching and diameter; VC volume scales with glomerular volume. **A/** Histogram of branch separation between 2nd order branches (A2 or E2) emerging from 1st order vessels (Con or E1). Branch intervals were assessed in 9 glomeruli, conduit vessels (Con, filled bars) are longer and less branched than 1st order efferent vessels (E1, open bars) (Mann Whitney U test medians (32.8, 15 μm), $P < 0.0001$). **B/** Histogram of 1st order vessel diameter coming off Vascular Chambers. Conduit vessels (filled bars) are significantly wider than Efferent first order vessels (open bars), efferent distribution is skewed towards lower values (15.3(12.8-18.9) v. 9.0(7.0-11.1); median(IQR); Mann Whitney U test, $p < 0.0001$). **C/** Afferent VC volume and **D/** Efferent VC volume scale with glomerular volume to a highly significant level ($R^2 = 0.517$ $P = 0.004$; $R^2 = 0.419$ $P = 0.012$ respectively). A minimum possible V_{AVC} and V_{EVC} (See Fig.3B) is also plotted to show V_G where VCs are a continuation of the attached arteriole (i.e. no VC widening).

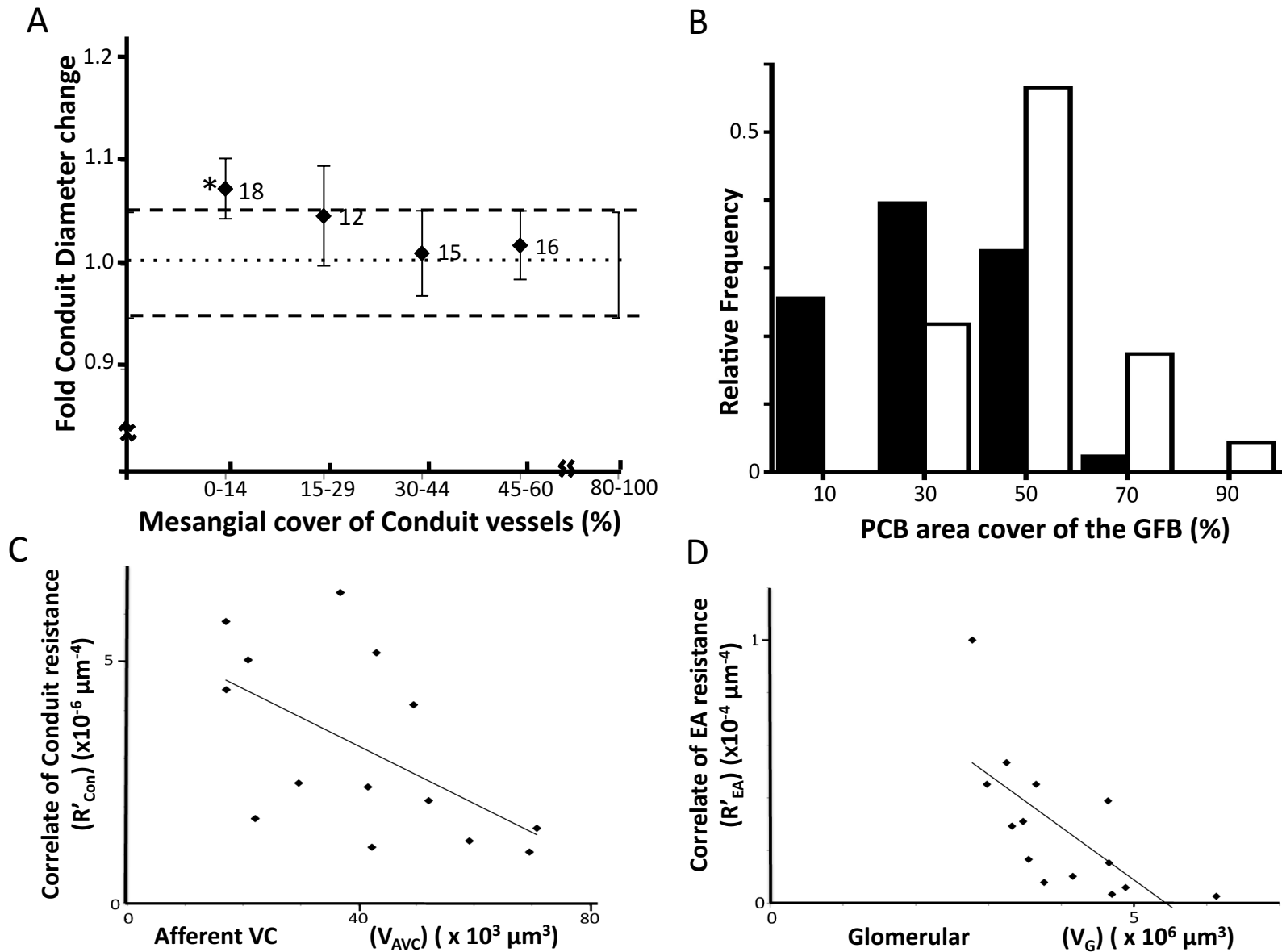
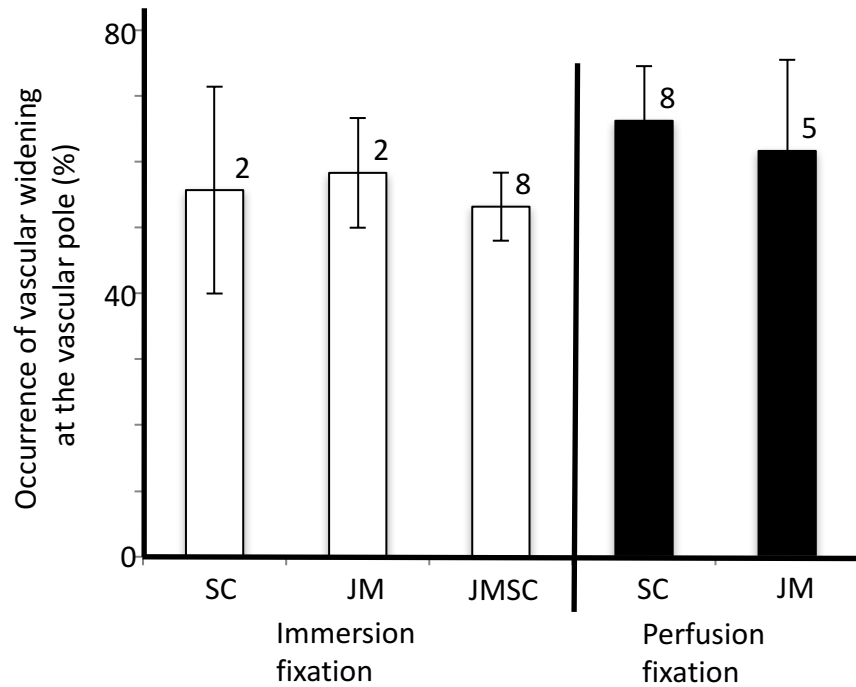


Figure 5. Conduit diameter changes with mesangium; conduit podocyte attachment; resistance v capacity examples **A/** Conduit diameter changes relative to mesangial cover. Conduit vessel diameters adjacent to the afferent VC with mesangial cover of 80-100% (GFB coverage 0-20%) were compared with diameters of low mesangial covered (distal) regions of the same vessel. The fold change in diameter shows a significant diameter increase of 7.4% (*) when mesangial cover is minimal (0-14% i.e. GFB 86-100%). Paired t-tests and Wilcoxon matched pair test ($P=0.04$). **B/** Histogram of podocyte cell body (PCB) area coverage of the filtration barrier of conduit vessels (filled bars) and small filtration capillaries (open bars). Conduits have significantly less PCB coverage of the GFB than filtration capillaries (ttest - $P<0.0001$). **C/** Conduit resistance versus Afferent VC volume. A significant negative correlation exists between a correlate of conduit resistance (R'_{con}) and afferent VC volume (V_{AVC}) ($R^2 = 0.327$, $P=0.033$). **D/** Efferent arteriole resistance per unit length (R'_{EA}) reduces in line with increasing V_G ($R^2 = 0.47$, $P=0.007$).

A



B

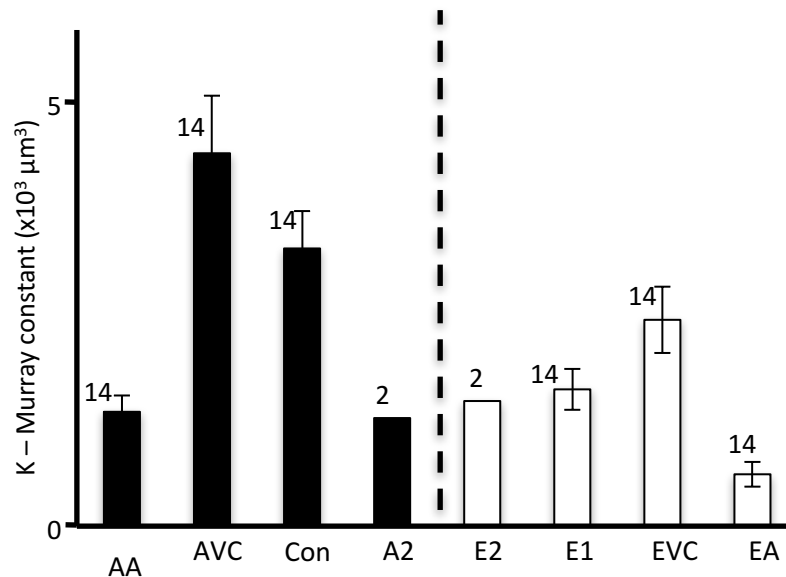


Figure 6. Vascular widenings in single sections. Murray constant from vascular radii A/

Observed occurrence of glomerular vascular widening in single sections. The frequency with which widening (implying VC presence) was observed at vascular poles in immersion and perfusion fixed glomeruli. SC - subcapsular glomeruli; JM - juxta-medullary glomeruli; JMSC - JM and SC glomeruli combined. (n = number of kidneys)

B/ In 14 glomeruli a Murray constant ($K = r^3 n_v$; where r is radius, n_v is vessel number; see text) was calculated for the afferent and efferent arteriolar tree leading through the VCs and thence into the 1st order vessels (Con and E1). In 2 glomeruli K was calculated for 2nd order vessels. The Murray relationship of equal K at each vessel level is absent in the AVC, EVC and conduit vessels.

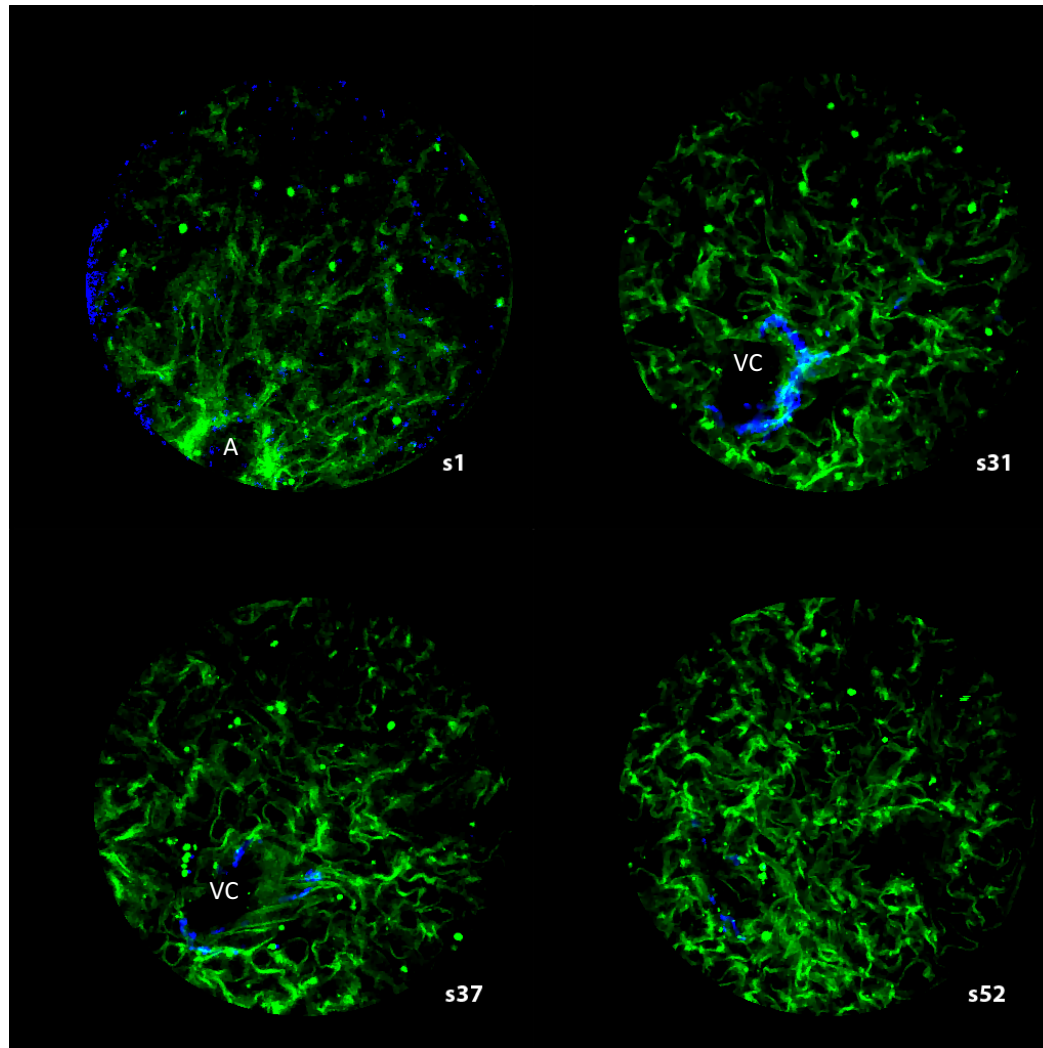


Figure 7. Multiphoton imaging of glomeruli. Images obtained by combining two photon fluorescence (TPF) signal images with second harmonic generation (SHG) images of an unfixed human glomerulus. The capillary walls emit a TPF signal (green) with most of the smaller filtration capillaries showing collapse. A banded Collagen signal (SHG blue) is located adjacent to a VC wall (intense Bowman's capsule Collagen has been blanked). Section s1 is close to the tissues physical surface; A - arteriole, (optical section 1 μ m deep). S31 shows a wide incomplete region of banded collagen around an uncollapsed region (VC) connected with A in s1. The banded collagen region has disappeared in s37 but offshoots in attached vessels appear in s37 (right of VC) and s52 (left of VC position). Diameter of field - 200 μ m. (See supplemental video S3 for full section series)

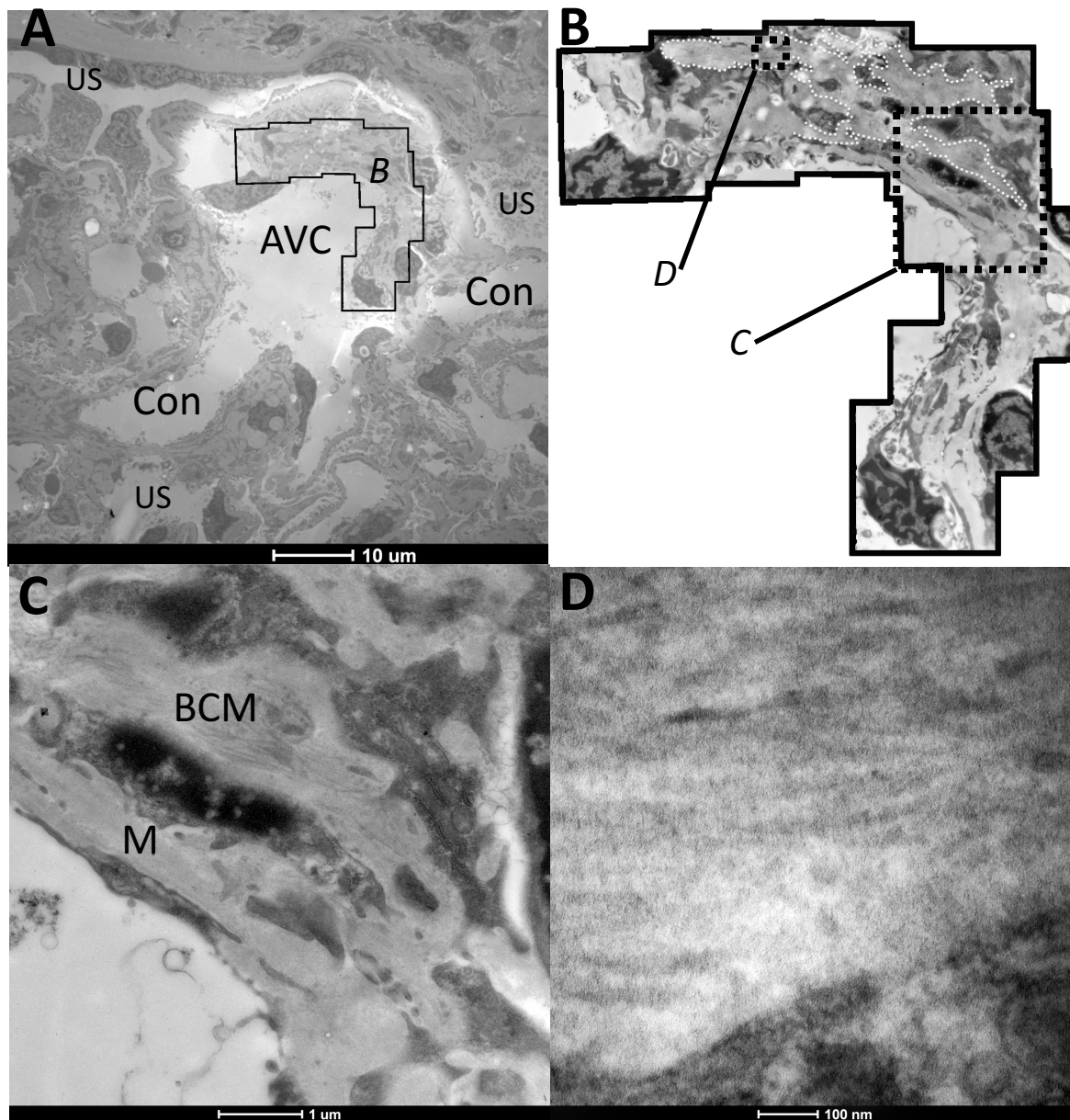


Figure 8. Transmission electron micrographs of Vascular chamber walls. Vascular Chamber were imaged using a Tecnai 12 electron microscope, low power **(A)** shows a vascular pole an AVC, conduit vessels (Con) and urinary space (US). **(B)** Montage of micrographs to show the disposition of the banded collagen fibres around the VC walls. White dotted lines show the extent of the mesangial matrix where banded collagen fibres were evident. **(C)** Area C from montage B with matrix rich in banded collagen (BCM) and where collagen is absent (M). **(D)** Area D from montage B with banded collagen fibres.

Table 1.	Afferent Arteriole AA	Afferent Vascular Chamber AVC			Afferent first order vessels Conduit vessels	
	diameter ($2 r_{AA}$) μm	min. diam. ($2 r'_{AVC}$) μm	Secn.depth diam. ($2 r''_{AVC}$) μm	max. diam. ($2 r'''_{AVC}$) μm	diameter ($2 r_{Con}$) μm	n_{Con}
mean	21.5	32.1	49.4	48.0	15.9	6.6
sem	1.2	1.5	3.4	3.6	0.7	0.6

Table 2.	Efferent Arteriole EA	Efferent Vascular Chamber EVC			Efferent first order vessels E1	
	diameter ($2 r_{EA}$) μm	min. diam. ($2 r'_{EVC}$) μm	Secn.depth diam. ($2 r''_{EVC}$) μm	max. diam. ($2 r'''_{EVC}$) μm	diameter ($2 r_{E1}$) μm	n_{E1}
mean	15.9	26.2	45.9	43.1	9.9	12.6
sem	1.2	1.4	9.1	4.3	0.4	1.4

Table 1 & 2. Afferent and efferent vascular diameters. Diameters of afferent and efferent vessels from resin embedded glomeruli (14) from 4 human kidneys. In all cases the afferent and efferent arterioles widen to form ellipsoidal chambers with between 2 and 11 high capacity conduit vessels emerging and conveying fluid away to the filtration capillaries. Blood from the filtration capillaries converges into 3 to 22 narrow efferent first order vessels which converge into the Efferent VC and thence the efferent arteriole. [In the 14 glomeruli analysed, 2 extra wide conduit vessels (19-24 μm) were found, 1 extrawide E1 drainage vessel (20-27 μm) but the branching was frequent as in other E1 vessels]. Vascular chamber dimensions: min.diam.; minimum diameter measured in the section plane avoiding oblique vessel sections. max.diam.; maximum diameter measured in the section plane avoiding oblique vessel sections. Secn. depth diam; diameter measured in the sectioning direction. sem; standard error of the mean

R_{AA}	V_{AVC}	R_{Con}	V_G	R_{E1}	V_{EVC}	R_{EA}

Table 3. Vascular resistance and capacity relationships. Significant correlations (8 out of 21) between 7 variables measured in human glomerular initial vasculature. Correlates of vascular resistance for afferent arterioles (R_{AA}), Conduit vessels (R_{Con}), first order efferent vessels (R_{E1}) and efferent arterioles (R_{EA}) were compared with each other and with AVC volume (V_{AVC}) glomerular volume (V_G) and EVC volume (V_{EVC}). + positive correlation, - negative correlation; * = $P < 0.05$, ** = $P \leq 0.01$; **** = $P \leq 0.0001$; § higher significance with outlier removed.

		AA	AA	AVC	AVC Coll.	Conduit	E1	EVC	EA	EA
		Diam. (μm)	Wall t (μm)	Diam. (μm)	Wall t (μm)	Diam. (μm)	Diam. (μm)	Diam. (μm)	Diam. (μm)	Wall. t (μm)
Fixed Resin Recon.	14G, 4K	21.5 \pm 1.2	6.6 \pm 0.3	43.2 \pm 2.8	*	15.9 \pm 0.7	9.9 \pm 0.4	38.4 \pm 4.9	15.9 \pm 1.2	3.0 \pm 0.1
Fixed Aq. Confocal	4G*, 1K	28.4 \pm 1.9	6.3 \pm 0.8	35.8 \pm 3.5	*	16.0 \pm 1.2	8.2	24.2	12.8	*
Fixed Aq. Multipho	3G*, 1K	*	*	50.2 \pm 3.7	4.2 \pm 0.8	12.8 \pm 1.6	6.9	28.1	7.4	*
Fresh Aq. Multipho	3G*, 2K	13.8	3.0	35.8 \pm 4.1	4.1 \pm 1.9	14.4 \pm 0.9	*	*	*	*
Fresh Aq. Multipho	Isolated1 G*, 1K	23.0	*	54.2	2.5	27.4	*	*	*	*

Table.4. Vascular diameters and wall thicknesses - all experiments. Comparison of AA, AVC, Conduit, E1, EVC, and EA measurements from resin section reconstruction with the same features in fixed and fresh glomeruli reconstructed from confocal and multiphoton microscope z stacks (SHG and TPF). EVC and AVC values have been averaged together for all 3 axes. AVC Collagen sheath (AVC Coll) enshrouded AVC and some parts of conduit vessels but scant evidence in EVC or E1 (multiphoton microscopy only). G and K indicate numbers of glomeruli and kidneys used. * not all quantities were observable and measureable.